statistically significant. All values are expressed as mean ± standard error of the mean (S.E.M., n = number).

2.13. *Ethical considerations*

All studies were performed in the laboratories of the Department of Diabetes and Clinical Nutrition, Kyoto University, in accordance with the Declaration of Helsinki.
The Animal Care Committee of Kyoto University Graduate School of Medicine approved animal care and procedures.

3. Results

3.1. *Effect of CRA on gluconeogenesis from lactate in rat liver perfusion*

The effect of CRA on gluconeogenesis was investigated in rat liver perfusion. Glucose output into the effluent perfusate was stabilized under 2 μmol/g/h. Upon changing perfusate from basal buffer to KRB containing 2 mM lactate, the glucose output rate increased rapidly and reached a steady state of approximately 10 μmol/g/h (Fig. 2). Glucose output rate was reduced by the addition of 100 μM CRA to the buffer, and continued to fall during the 20 min perfusion with CRA. After 100 μM CRA perfusion, the glucose output rate was 7.3 ± 0.3 μmol/g liver/h, approximately 73% of that before CRA perfusion. Glucose output gradually recovered after washout of CRA with glucose-free KRB containing 2 mM lactate, and, after washout of lactate, fell to under 2 μmol/g/h. Average glucose output rate during the last 14 min of the 20 min perfusion (66–80 min) with KRB containing 20–100 μM CRA was then measured and compared to control (Fig. 3). The glucose output was significantly

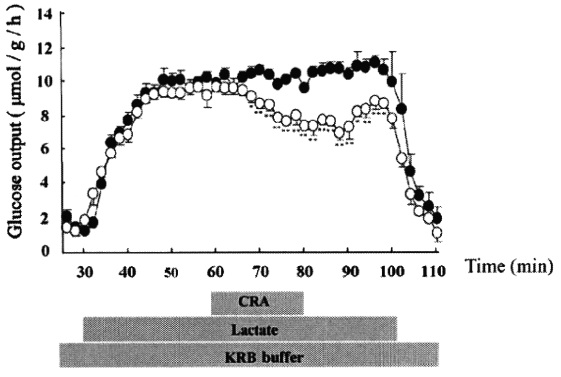

Fig. 2 – Inhibitory effect of CRA on glucose output rate in perfused rat liver. Liver was perfused with glucose-free KRB buffer for 110 min, and from 30 to 100 min with glucose-free buffer containing 2 mM lactate. From 60 to 80 min, perfusion was with buffer containing 2 mM lactate and with 100 μM CRA. From 100 to 110 min, perfusion was with glucose-free KRB buffer without lactate. Effluent perfusate was collected every 2 min, and glucose content was measured. CRA (○), control (●). Data are shown as means with S.E.M. (n = 5 for each group). *P < 0.05, **P < 0.01 compared with the value of control.

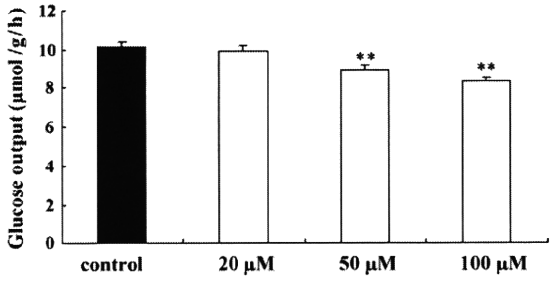

Fig. 3 – Effect of CRA on glucose output rate in perfused rat liver. Liver was perfused as in Fig. 2. Average glucose output rate during the last 14 min (66–80 min) perfusion period with buffer containing 20–100 μM CRA was compared. CRA (□), control (■). Data are shown as means with S.E.M. (n = 5 for each group). **P < 0.01 compared with the value of control.

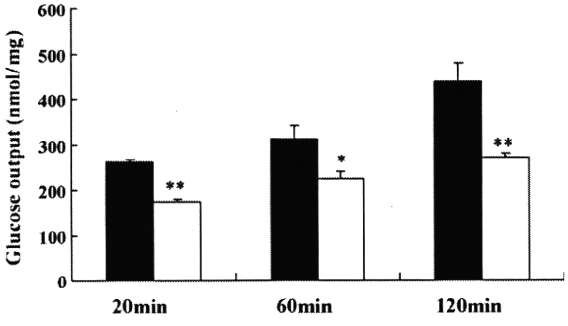

Fig. 4 – Time course of the inhibitory effect of CRA on gluconeogenesis in isolated hepatocytes. Hepatocytes were incubated at 37 °C in a humidified atmosphere (5% CO_2) of DMEM without glucose but containing 1 mM lactate and 0.24 mM IBMX in the presence of 100 μM CRA or vehicle for 20, 60, and 120 min. Glucose content in supernatant was measured by glucose oxidation method. CRA (□), control (■). Data are shown as means with S.E.M. (n = 8 for each group). *P < 0.05, **P < 0.01 compared with the value of control.

reduced by the addition of 50 μM (12%) and 100 μM (18%) of CRA compared to control (P < 0.01), dose-dependently in the 20–100 μM CRA range.

3.2. *Effect of CRA on gluconeogenesis from lactate in isolated hepatocytes*

The effect of CRA on gluconeogenesis from lactate was investigated in hepatocytes. Fig. 4 shows the time course of inhibition by CRA of hepatic gluconeogenesis from lactate. The gluconeogenesis from lactate increased in a time-dependent manner linearly up to 120 min, indicating that the metabolic flow in the hepatocytes was at a steady state both in the presence and in the absence of CRA. After 20, 60, and 120 min exposure to 100 μM CRA, hepatic gluconeogenesis was significantly inhibited compared to control. The gluconeogenesis

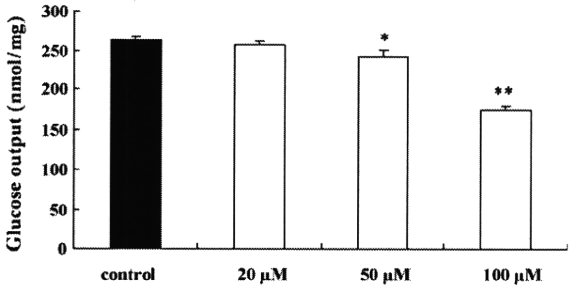

Fig. 5 – Concentration-dependence of the inhibitory effect of CRA on gluconeogenesis in isolated hepatocytes. Hepatocytes were incubated at 37 °C in a humidified atmosphere (5% CO_2) of DMEM without glucose but containing 1 mM lactate and 0.24 mM IBMX in the presence of 20–100 μM CRA or vehicle for 20 min. Glucose content in supernatant was measured by glucose oxidation method. CRA (□), control (■). Data are shown as means with S.E.M. ($n = 9$ for each group). *$P < 0.05$, **$P < 0.01$ compared with the value of control.

in hepatocytes decreased in a dose-dependent manner after 20 min incubation with CRA (Fig. 5).

3.3. *Effect of CRA on neosynthesized [^{14}C]-glucose in isolated hepatocytes*

The effect of CRA on gluconeogenesis from [^{14}C]-pyruvate in the presence of 10 mM glucose in culture medium was investigated in isolated hepatocytes. Fig. 6 shows the time course of inhibition by CRA of hepatic gluconeogenesis from [^{14}C]-pyruvate. The gluconeogenesis from [^{14}C]-pyruvate increased in a time-dependent manner linearly up to 120 min, indicating that the metabolic flow in the

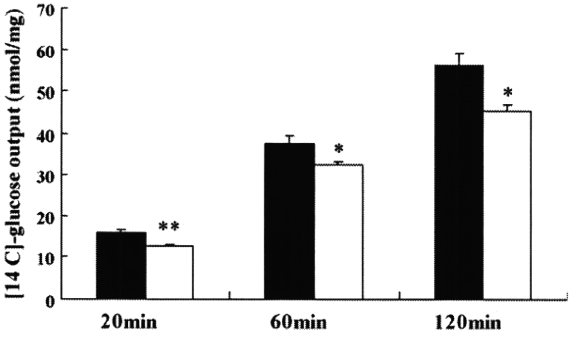

Fig. 6 – Time course of the inhibitory effect of CRA on neosynthesized [^{14}C]-glucose in isolated hepatocytes. Hepatocytes were incubated at 37 °C in a humidified atmosphere (5% CO_2) in DMEM with 10 mM glucose, 1 mM pyruvate and 0.24 mM IBMX, and 0.05 μCi of [^{14}C]-pyruvate in the presence of 100 μM CRA or vehicle for 20, 60, and 120 min. Radioactivity was measured by liquid scintillation counter. CRA (□), control (■). Data are shown as means with S.E.M. ($n = 4$ for each group). *$P < 0.05$, **$P < 0.01$ compared with the value of control.

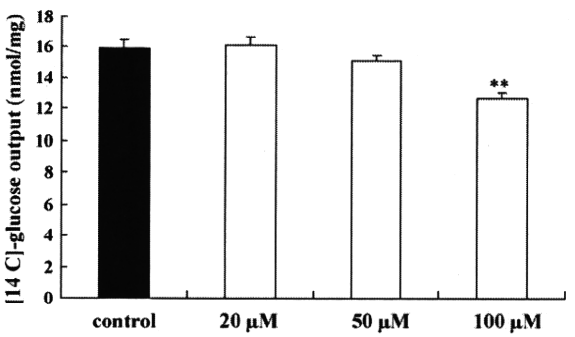

Fig. 7 – Concentration dependence of the inhibitory effect of CRA on neosynthesized [^{14}C]-glucose in isolated hepatocytes. Hepatocytes were incubated at 37 °C in a humidified atmosphere (5% CO_2) in DMEM with 10 mM glucose, 1 mM pyruvate and 0.24 mM IBMX, and 0.05 μCi of [^{14}C]-pyruvate in the presence of 20–100 μM CRA or vehicle for 20 min. Radioactivity was measured by liquid scintillation counting. CRA (□), control (■). Data are shown as means with S.E.M. ($n = 4$ for each group). **$P < 0.01$ compared with the value of control.

hepatocytes was at a steady state both in the presence and in the absence of CRA. After 20, 60, and 120 min exposure to 100 μM CRA, hepatic gluconeogenesis was significantly inhibited compared to control. The gluconeogenesis from [^{14}C]-pyruvate decreased in a dose-dependent manner after 20 min incubation with CRA (Fig. 7). Thus, CRA inhibited hepatic gluconeogenesis in the presence of 10 mM glucose as well as in the absence of glucose in culture medium.

3.4. *Effect of CRA on F-2,6-BP production in isolated hepatocytes*

The effect of CRA on the production of F-2,6-BP was examined in isolated hepatocytes. Hepatocytes were incubated in glucose-free medium with 100 μM CRA for 20 min, and the F-2,6-BP was then measured. CRA increased F-2,6-BP production in hepatocytes approximately 2-fold compared to control ($P < 0.05$) (Fig. 8). Next, hepatocytes were incubated in 10 mM glucose with 100 μM CRA for 20 min, and the F-2,6-BP was then measured. The addition of 10 mM glucose doubled the basal F-2,6-BP. In the presence of 10 mM glucose, CRA again increased F-2,6-BP production in hepatocytes approximately 1.5-fold compared to control, clearly indicating the central role of cellular F-2,6-BP levels in CRA inhibition of gluconeogenesis ($P < 0.01$) (Fig. 8).

3.5. *Effect of CRA on intracellular cAMP level in isolated hepatocytes*

To further clarify the mechanism of action of CRA, we compared the intracellular cAMP levels in isolated hepatocytes. CRA reduced the cAMP level in hepatocytes after incubation for 20 min ($P < 0.05$) (Fig. 9A). Forskolin, which activates the catalytic subunit of adenylate cyclase, evoked a

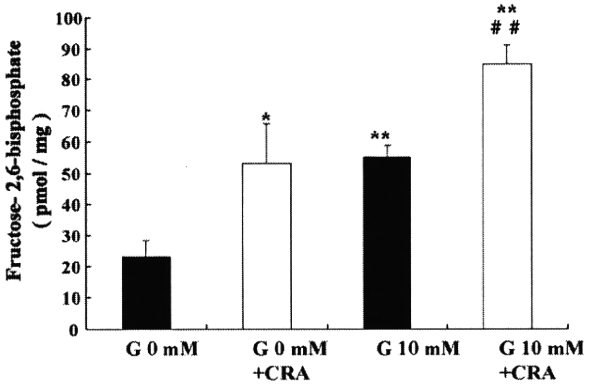

Fig. 8 – Effect of CRA on F-2,6-BP production in isolated hepatocytes. Hepatocytes were incubated at 37 °C in a humidified atmosphere (5% CO_2) in DMEM with or without 10 mM glucose (G) but containing 1 mM lactate and 0.24 mM IBMX in the presence of 100 μM CRA or vehicle for 20 min. CRA (□), control (■). Data are shown as means with S.E.M. (n = 5–7 for each group). *P < 0.05, **P < 0.01 compared to the value of control without glucose. ##P < 0.01 compared to the value control with 10 mM glucose.

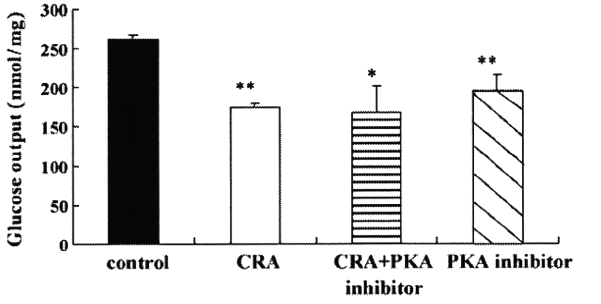

Fig. 10 – Effect of CRA on gluconeogenesis with a PKA inhibitor (H89) in isolated hepatocytes. Hepatocytes were incubated at 37 °C in a humidified atmosphere (5% CO_2) in DMEM without glucose but containing 1 mM lactate, 0.24 mM IBMX with/without 10 μM H89 in the presence of 100 μM CRA or vehicle for 20 min. Glucose content in supernatant was measured by glucose oxidation method. CRA (□), control (■), CRA + PKA inhibitor (▤), PKA inhibitor (▨). Data are shown as means with S.E.M. (n = 9 for each group). *P < 0.05, **P < 0.01 compared with the value of control.

marked elevation of the cAMP level after incubation for 20 min. CRA also reduced the forskolin-evoked increment of the cAMP level after incubation for 20 min ($P < 0.05$) (Fig. 9B).

3.6. *Effect of CRA on gluconeogenesis with cAMP-dependent protein kinase (PKA) inhibitor in isolated hepatocytes*

Hepatic gluconeogenesis in isolated hepatocytes was inhibited after 20 min exposure to the PKA inhibitor, N-[2-(*p*-bromocinnamylamino)ethyl]-5-isoquinolinesulfonamide (H89) at the concentration of 10 μM (Fig. 10). We also evaluated the effect of CRA on gluconeogenesis in hepatocytes in the presence of 10 μM H89. The PKA inhibitor did not have an additive inhibitory effect on CRA-induced inhibition of gluconeogenesis.

3.7. *Effects of CRA on GK activity and G6Pase activity in isolated hepatocytes*

The level of F-2,6-BP is regulated by the synthesizing (6-phosphofructo-2-kinase, PFK-2) and the degrading (fructose-2,6-bisphosphatase, F-2,6-BPase) enzyme complex. In insulin-producing cells, PFK-2/F-2,6-BPase reportedly interacts with GK, and the overexpression of PFK-2/F-2,6-BPase increases GK activity. In this study, CRA was found to increase the level of F-2,6-BP in isolated hepatocytes. Therefore, we measured GK activity after exposure to CRA. Hepatocytes were incubated with 100 μM CRA for 20 min, and GK activity was then measured. CRA significantly increased GK activity compared to control (control: 0.82 ± 0.04, n = 5, CRA: 1.09 ± 0.02 nmol/mg protein/min, n = 5; $P < 0.01$).

Since G6Pase is also a rate-limiting enzyme of gluconeogenesis, we measured G6Pase activity after exposure to CRA.

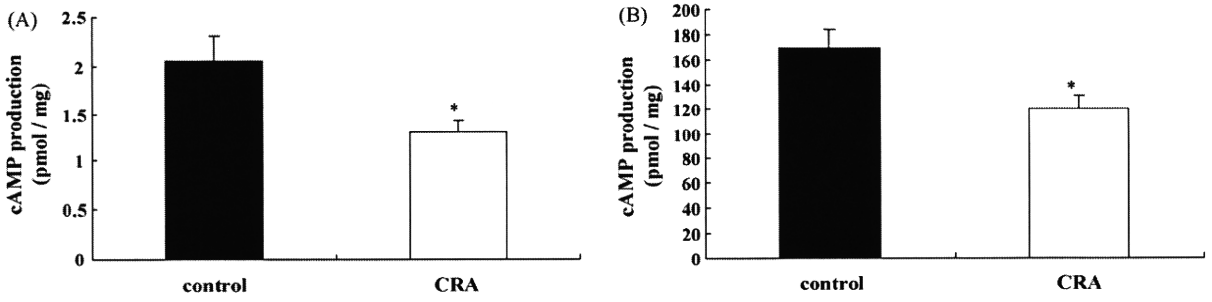

Fig. 9 – Effect of CRA on cAMP level in isolated hepatocytes. Hepatocytes were incubated at 37 °C in a humidified atmosphere (5% CO_2) in DMEM without glucose but containing 1 mM lactate and 0.24 mM IBMX without (A) or with (B) 5 μM forskolin in the presence of 100 μM CRA or vehicle for 20 min. CRA (□), control (■). Data are shown as means with S.E.M. (n = 4–6 for each group). *P < 0.05 compared with the value of control.

Hepatocytes were incubated with 100 μM CRA for 20 min, and G6Pase activity was then measured. CRA did not alter G6Pase activity (control: 140 ± 22, $n = 5$, CRA: 168 ± 37 nmol/mg protein/min, $n = 5$; $P = 0.55$).

4. Discussion

This is the first study to demonstrate that CRA reduces hepatic glucose production. We showed that CRA decreases gluconeogenesis in perfused rat liver in a dose-dependent manner (20–100 μM). We also showed that CRA decreases gluconeogenesis in isolated hepatocytes both in glucose-free medium and in glucose-containing medium in a dose-dependent manner (20–100 μM).

To determine whether the CRA concentration used in this study is physiologically relevant, we measured CRA in the blood after oral administration in dog. When CRA was orally administered at 20 mg/kg of body weight in dog, the concentration in peripheral blood was 17 μM after 90 min (unpublished data). In this study, CRA was found to inhibit hepatic gluconeogenesis at a concentration about 5-fold higher than that used in dog. Considering that the concentration of CRA in the portal vein should be higher than that in the peripheral vein when orally administered, the dosage of CRA used in these experiments seems appropriate.

To investigate the mechanism of action of CRA, we measured its effect on the production of F-2,6-BP, which plays an important role in the regulation of both glycolysis and gluconeogenesis. F-2,6-BP is a potent physiological activator of PFK-1, the rate-limiting enzyme in glycolysis [21,22], and inhibits fructose-1,6-bisphosphatase (F-1,6-BPase), an enzyme active in gluconeogenesis [23,24] (Fig. 11). In this study, CRA was found to markedly enhance the F-2,6-BP production during lactate-stimulated gluconeogenesis. Thus, CRA-induced increase in F-2,6-BP stimulates glycolysis and inhibits gluconeogenesis.

The activity of the synthesizing (PFK-2) and the degrading (F-2,6-BPase) enzyme of F-2,6-BP is determined by the phosphorylation state of PKA. Activation of PFK-2 is known to elevate cellular levels of F-2,6-BP, and cAMP inactivates PFK-2 activity through PKA in hepatocytes. On the other hand, cAMP activates F-2,6-BPase through PKA in hepatocytes [25]. In this study, we found that CRA decreases the cAMP level in isolated hepatocytes, suggesting that CRA increases F-2,6-BP by lowering intracellular cAMP level. We also found that a PKA inhibitor (H89) decreased gluconeogenesis in isolated hepatocytes, but did not have an additive inhibitory effect on CRA-induced inhibition of gluconeogenesis. Thus, CRA would seem to inhibit hepatic gluconeogenesis through the PKA-mediated pathway. However, CRA was found to reduce the forskolin-evoked increment of intracellular cAMP level. Thus, the mechanism by which CRA decreases the intracellular cAMP level must be investigated in further study.

Recently, Massa et al. [26] reported that PFK-2/F-2,6-BPase enzyme complex interacts with GK in the insulin-producing cells and that overexpression of PFK-2/F-2,6-BPase increases GK activity. In this study, we measured GK activity after exposure to CRA in isolated hepatocytes. CRA was found to increase GK activity, leading to glycolysis in the hepatocytes. On the other hand, Wen et al. [9] reported that CRA inhibited glycogen phospholylase *a* purified from rat liver. This direct effect of CRA on the enzyme of glycogen phospholylase suggests that CRA might inhibit glycogenolysis, another pathway to glucose production besides gluconeogenesis. Thus, the increased glycolysis and decreased glycogenolysis in hepatocytes may also contribute to the anti-diabetic action of CRA.

It was previously shown that Banaba leaf extract (1% CRA) decreases blood glucose levels in humans in a dose-dependent manner [27]. In addition, CRA has been shown to reduce post

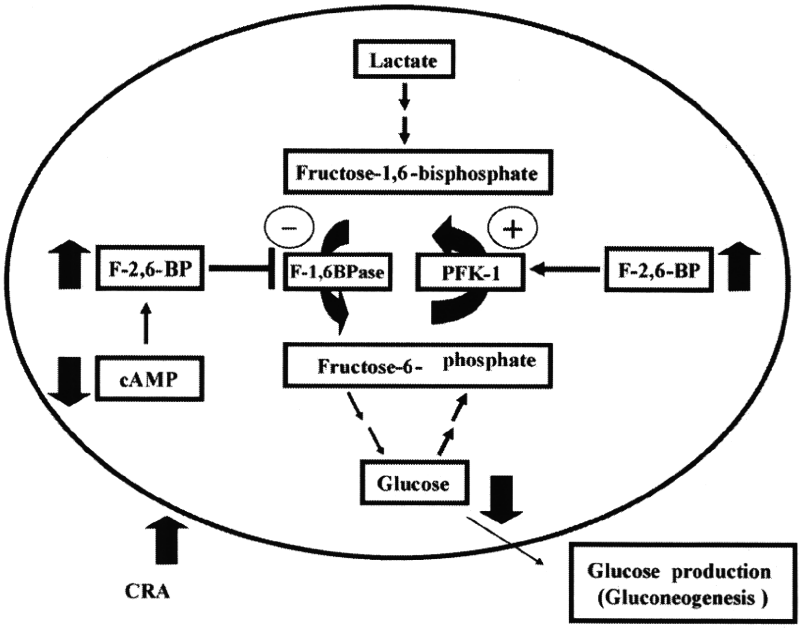

Fig. 11 – Mechanism of inhibitory action of CRA on gluconeogenesis.

challenge plasma glucose levels in human [11]. Considered together, these data suggest that CRA may provide a valuable new therapy in the treatment of type 2 diabetes.

Acknowledgments

This study was supported in part by Grants-in-Aids for Scientific Research from the Ministry of Education, Culture, Sports, Science and Technology of Japan; Health and Labour Sciences Research Grants for Research on Human Genome, Tissue Engineering, and Food Biotechnology from the Ministry of Health, Labor and Welfare of Japan; and Health and Labour Sciences Research Grants for Comprehensive Research on Aging and Health from the Ministry of Health, Labor and Welfare of Japan.

Conflict of interest

The authors state that they have no conflicts of interest.

REFERENCES

[1] E. Quisumbing, Medicinal Plants of the Phillippines, Katha Publishing, Quezon City, 1978, pp. 640–642.
[2] N. Banno, T. Akihisa, H. Tokuda, K. Yasukawa, H. Higashihara, M. Ukiya, et al., Triterpene acids from the leaves of Perilla frutescens and their anti-inflammatory and antitumor-promoting effects, Biosci. Biotechnol. Biochem. 68 (2004) 85–90.
[3] M. Yoshida, M. Fuchigami, T. Nagao, H. Okabe, K. Matsunaga, J. Takata, et al., Antiproliferative constituents from Umbelliferae plants VII. Active triterpenes and rosmarinic acid from Centella asiatica, Biol. Pharm. Bull. 28 (2005) 173–175.
[4] K.S. Ahn, M.S. Hahm, E.J. Park, H.K. Lee, I.H. Kim, Corosolic acid isolated from the fruit of Crataegus pinnatifida var. psilosa is a protein kinase C inhibitor as well as a cytotoxic agent, Planta Med. 64 (1998) 468–470.
[5] D.H. Kim, K.M. Han, I.S. Chung, D.K. Kim, S.H. Kim, B.M. Kwon, et al., Triterpenoids from the flower of Campsis grandiflora K. Schum. as human acyl-CoA: cholesterol acyltransferase inhibitors, Arch. Pharm. Res. 28 (2005) 550–556.
[6] N.T. Dat, X.F. Cai, M.C. Rho, H.S. Lee, K. Bae, Y.H. Kim, The inhibition of diacylglycerol acyltransferase by terpenoids from Youngia koidzumiana, Arch. Pharm. Res. 28 (2005) 164–168.
[7] C. Murakami, K. Myoga, R. Kasai, K. Ohtani, T. Kurokawa, S. Ishibashi, et al., Screening of plant constituents for effect on glucose transport activity in Ehrlich ascites tumour cells, Chem. Pharm. Bull. (Tokyo) 41 (1993) 2129–2131.
[8] T. Miura, Y. Itoh, T. Kaneko, N. Ueda, T. Ishida, M. Fukushima, et al., Corosolic acid induces GLUT4 translocation in genetically type 2 diabetic mice, Biol. Pharm. Bull. 27 (2004) 1103–1105.
[9] X. Wen, H. Sun, J. Liu, G. Wu, L. Zhang, X. Wu, et al., Pentacyclic triterpenes. Part 1: the first examples of naturally occurring pentacyclic triterpenes as a new class of inhibitors of glycogen phosphorylases, Bioorg. Med. Chem. Lett. 15 (2005) 4944–4948.
[10] T. Miura, N. Ueda, K. Yamada, M. Fukushima, T. Ishida, T. Kaneko, et al., Antidiabetic effects of corosolic acid in KK-Ay diabetic mice, Biol. Pharm. Bull. 29 (2006) 585–587.
[11] M. Fukushima, F. Matsuyama, N. Ueda, K. Egawa, J. Takemoto, Y. Kajimoto, et al., Effect of corosolic acid on postchallenge plasma glucose levels, Diabetes Res. Clin. Pract. 73 (2006) 174–177.
[12] A. Consoli, Role of liver in pathophysiology of NIDDM, Diabetes Care 15 (1992) 430–441.
[13] E. Ferrannini, L.C. Groop, Hepatic glucose production in insulin-resistant states, Diabetes Metab. Rev. 5 (1989) 711–726.
[14] T. Sugano, K. Suda, M. Shimada, N. Oshino, Biochemical and ultrastructural evaluation of isolated rat liver systems perfused with a hemoglobin-free medium, J. Biochem. (Tokyo) 83 (1978) 995–1007.
[15] Y. Nishimura, Y. Inoue, H. Takeuchi, Y. Oka, Acute effects of pioglitazone on glucose metabolism in perfused rat liver, Acta. Diabetol. 34 (1997) 206–210.
[16] M. Hosokawa, B. Thorens, Glucose release from GLUT2-null hepatocytes: characterization of a major and a minor pathway, Am. J. Physiol. Endocrinol. Metab. 282 (2002) E794–E801.
[17] E. Van Schaftingen, B. Lederer, R. Bartrons, H.G. Hers, Fructose-2,6-bisphosphatase from rat liver, Eur. J. Biochem. 124 (1982) 143–149.
[18] I. Miwa, Y. Mita, T. Murata, J. Okuda, M. Sugiura, Y. Hamada, Utility of 3-O-methyl-N-acetyl-D-glucosamine, an N-acetylglucosamine kinase inhibitor, for accurate assay of glucokinase in pancreatic islets and liver. Enzyme Protein 48 (1994–1995) 135–142.
[19] K. Aoki, T. Saito, S. Satoh, K. Mukasa, M. Kaneshiro, S. Kawasaki, et al., Dehydroepiandrosterone suppresses the elevated hepatic glucose-6-phosphatase and fructose-1,6-bisphosphatase activities in C57BL/Ksj-db/db mice: comparison with troglitazone, Diabetes 48 (1999) 1579–1585.
[20] J.V. Passoneau, O.H. Lowry, Enzymic Analysis: A Practical Guide, Humana Press, Totowa, 1993.
[21] E. Van Schaftingen, L. Hue, H.G. Hers, Fructose 2,6-bisphosphate, the probably structure of the glucose- and glucagon-sensitive stimulator of phosphofructokinase, Biochem. J. 192 (1980) 897–901.
[22] S.J. Pilkis, M.R. El-Maghrabi, J. Pilkis, T.H. Claus, D.A. Cumming, Fructose 2,6-bisphosphate. A new activator of phosphofructokinase, J. Biol. Chem. 256 (1981) 3171–3174.
[23] E. Van Schaftingen, B. Lederer, R. Bartrons, H.G. Hers, A kinetic study of pyrophosphate: fructose-6-phosphate phosphotransferase from potato tubers, Application to a microassay of fructose 2,6-bisphosphate, Eur. J. Biochem. 129 (1982) 191–195.
[24] E. Van Schaftingen, H.G. Hers, Inhibition of fructose-1,6-bisphosphatase by fructose 2,6-biphosphate, Proc. Natl. Acad. Sci. U.S.A. 78 (1981) 2861–2863.
[25] S.J. Pilkis, M.R. el-Maghrabi, T.H. Claus, Hormonal regulation of hepatic gluconeogenesis and glycolysis, Annu. Rev. Biochem. 57 (1988) 755–783.
[26] L. Massa, S. Baltrusch, D.A. Okar, A.J. Lange, S. Lenzen, M. Tiedge, Interaction of 6-phosphofructo-2-kinase/fructose-2, 6-bisphosphatase (PFK-2/FBPase-2) with glucokinase activates glucose phosphorylation and glucose metabolism in insulin-producing cells, Diabetes 53 (2004) 1020–1029.
[27] W.V. Judy, S.P. Hari, W.W. Stogsdill, J.S. Judy, Y.M. Naguib, R. Passwater, Antidiabetic activity of a standardized extract (Glucosol) from Lagerstroemia speciosa leaves in type II diabetics. A dose-dependence study, J. Ethnopharmacol. 87 (2003) 115–117.

Endocrine Journal 2010, **57** (6), 509-516

ORIGINAL

Phenotypical variety of insulin resistance in a family with a novel mutation of the insulin receptor gene

Ikuko Takahashi[1], Yuichiro Yamada[2], Hiroko Kadowaki[3,4], Momoko Horikoshi[4], Takashi Kadowaki[4], Takuma Narita[2], Satoko Tsuchida[1], Atsuko Noguchi[1], Akio Koizumi[5] and Tsutomu Takahashi[1]

[1] *Department of Pediatrics, Akita University Graduate School of Medicine, Akita, Japan*
[2] *Department of Endocrinology, Diabetes and Geriatric Medicine, Akita University Graduate School of Medicine, Akita, Japan*
[3] *Department of Child Studies, Kasei-Gakuin University, Tokyo, Japan*
[4] *Department of Metabolic Diseases, Graduate School of Medicine, University of Tokyo, Tokyo, Japan*
[5] *Department of Health and Environmental Sciences, Graduate School of Medicine, Kyoto University, Kyoto, Japan*

Abstract. A novel mutation of insulin receptor gene (INSR gene) was identified in a three generation family with phenotypical variety. Proband was a 12-year-old Japanese girl with type A insulin resistance. She showed diabetes mellitus with severe acanthosis nigricans and hyperinsulinemia without obesity. Using direct sequencing, a heterozygous nonsense mutation causing premature termination at amino acid 331 in the α subunit of INSR gene (R331X) was identified. Her father, 40 years old, was not obese but showed impaired glucose tolerance. Her paternal grandmother, 66 years old, has been suffered from diabetes mellitus for 15 years. Interestingly, they had the same mutation. One case of leprechaunism bearing homozygous mutation at codon 331 was identified. These findings led to the hypothesis that R331X may contribute to the variation of DM in the general population in Japan. An extensive search was done in 272 participants in a group medical examination that included 92 healthy cases of normoglycemia and 180 cases already diagnosed type 2 DM or detected hyperglycemia. The search, however, failed to detect any R331X mutation in this local population. In addition, the proband showed low level C-peptide/insulin molar ratio, indicating that this ratio is considered to be a useful index for identifying patients with genetic insulin resistance. In conclusion, a nonsense mutation causing premature termination after amino acid 331 in the α subunit of the insulin receptor was identified in Japanese diabetes patients. Further investigations are called for to address the molecular mechanism.

Key words: Insulin receptor, Insulin resistance, Type 2 diabetes, Leprechaunism, C-peptide/insulin molar ratio

THE INTERACTION of insulin with its cell surface receptor is the first step in insulin action and the first identified target of insulin resistance. Mutations in the insulin receptor gene lead to the insulin resistance in several syndromic forms. The human insulin receptor is encoded by a single gene with 22 exons and is an assembly of a disulfide bond-linked tetramer composed of two α and two β subunits [1-5]. After binding of insulin to the extracellular α subunit, the tyrosine kinase of the membrane spanning β subunit is activated and the receptor is autophosphorylated [6]. Insulin receptor kinase regulates the action of insulin on metabolism and growth through signal transduction pathways and is therefore thought to be central to insulin action [7].

Some dozens of mutations in the human insulin receptor gene have already been identified to date [8-11]. Homozygous or compound-heterozygous mutations in the insulin receptor gene are found in patients with syndromes of severe insulin resistance [12]. More severe Donohue syndrome ("Leprechaunism" OMIM 246200) and the milder Rabson-Mendenhall syndrome (OMIM 262190) are characterized by intrauterine and postnatal growth retardation, facial dysmorphism, lack of subcutaneous fat and altered glucose homeostasis with hyperinsulinemia, acanthosis nigricans and reduced life expectancy [13-15]. Cells from most patients with Donohue syndrome show absent or

Received Nov. 25, 2009; Accepted Feb. 18, 2010 as K09E-339
Released online in J-STAGE as advance publication Mar. 25, 2010

Correspondence to: Ikuko Takahashi, M.D., Department of Pediatrics, Akita University Graduate School of Medicine, Hondo 1-1-1, Akita-shi, Akita, 010-8543, Japan.
E-mail takaiku@doc.med.akita-u.ac.jp

severely reduced insulin binding, whereas those with Rabson-Mendenhall retain some insulin binding capacity. Therefore, it has been proposed that severity of the phenotype is determined by the degree of insulin resistance and that residual insulin binding capacity correlates with survival. Heterozygous mutations in the insulin receptor gene have been demonstrated in type A insulin resistance with the triad of insulin resistance, acanthosis nigricans, and hyperandrogenism (OMIM147670) [16].

In this study, we identified a heterozygous mutation causing premature termination at amino acid 331 substituting a termination codon for arginine in the L2 domain in α subunit of the insulin receptor gene in a Japanese patient with diabetes mellitus and hyperinsulinemia. Interestingly, her family members shared the same mutation but showed different clinical course.

Materials and Methods

Subjects

The proband, a girl of 12 years old, was referred to our hospital because of glucosuria detected by school urinary screening. She presented with mild symptoms of polydipsia and polyuria. She was born to unrelated Japanese parents at 37 weeks of gestation (birth weight 2495 g, birth length 48 cm). At birth, she did not have the dysmorphic features characteristic of leprechaunism or Rabson-Mendenhall syndrome, including intrauterine growth retardation, fasting hypoglycemia. Sensorineural hearing loss in right side was diagnosed when she was infant, but did not deteriorate.

At presentation, she was not obese, but showed severe acanthosis nigricans with scratching scar of her neck. It also mildly existed at the axilla and elbow. Hirsutism was not observed. Body mass index (BMI) was 21.6 (height 148.6 cm, weight 47.7 kg). Blood pressure was 110/70 mmHg. Pubertal stage was B2 and PH1. Laboratory tests revealed the following; HbA1c, 9.2 %; FPG, 124 mg/dL; IRI, 65.7 μU/mL; C-peptide, 3.18 ng/mL; AST, 20 IU/L; ALT, 18 IU/L; total cholesterol, 194 mg/dL; HDL cholesterol, 43.7 mg/dL; testosterone, 0.33 ng/mL. Islet associated autoantibodies were absent. Urine testing showed no ketonuria but proteinuria (microalbumin 64.4mg/g cr) and glucosuria. Ocular complication and retinopathy was not detected. Abdominal CT revealed no fatty liver and area of visceral fat on umbilical level was 41.8 cm^2 (normal: 60>). Although she showed diabetes mellitus with severe insulin resistance, her data of body composition was not suggested risk for obesity or metabolic syndrome. Self monitored blood glucose levels were 120-140 mg/dL at premeal time and 170-200 mg/dL at postprandial time. Her father, 40 years old, was healthy and no obesity (BMI 21.8) from a clinical point of view at the time of investigation. Her paternal grandmother, 66 years old, has been suffered from diabetes mellitus. She was also not obese (BMI 21.6) and has been treated with sulfonylureas for 15-years. She already developed retinopathy and presented vitreous hemorrhage 10 years ago. Her younger brother, seven years of age, had mild mental retardation and supported by special education. He showed mild obesity but normal response to oral glucose tolerance test without hyperinsulinemia (FPG, 86 mg/dL; IRI, 8.6 μU/mL; C-peptide, 1.53 ng/mL).

Measurements

The standard 75 g oral glucose tolerance test (OGTT) was performed, after overnight fast. Levels of glucose, insulin and C-peptide were measured at 0, 30, 60, 90 and 120 min. Insulin was measured using an enzyme immunoassay (E test TOSOH II; TOSOH Corporation, Tokyo, Japan). Cross-reactivity with proinsulin was 2 %. C-peptide was measured using a chemiluminescent enzyme immunoassay (LUMIPULSE Presto C-peptide; FUJIREBIO Inc., Tokyo, Japan). Proinsulin was measured using a RIA2 antibody method (HUMAN PROINSULIN RIA KIT; Linco Research Inc., St. Charles, MO).

We calculated C-peptide/insulin molar ratio from each molecular weight and international unit of insulin i.e. 26 IU/mg. We estimated molecular weight of insulin at 5800 and C-peptide at 3600. Consequently, 1 μU/mL of insulin is 6.09 pmol/L and 1 ng/mL of C-peptide is 0.278 nmol/L.

Sequence analysis

Informed consent was obtained from her family. Genomic DNA was extracted from peripheral blood lymphocytes using a DNA isolation kit for mammalian blood. Exon 1-2 of the insulin gene and Exons 1-22 of the insulin receptor gene were individually amplified using primer sets as described [17, 18]. PCR products were purified for direct sequence analysis on an ABI gene analyzer 310 or 3100 system according to the manufacturer's instructions (Applied Biosystems).

Analysis for prevalence of R331X mutant in population

We tested the frequency of R331X in type 2 DM or by chance hyperglycemia in adult people, living in the Akita prefecture located in northern Japan. We studied 272 participants of a group medical examination, comprised 92 healthy cases checked normoglycemia and 180 cases already diagnosed type 2 DM or detected hyperglycemia. These included 47 cases with family history of DM and 14 cases diagnosed before third decade. All participants gave informed consent, and the Ethics Committee of Kyoto University School of Medicine approved the study.

Genotyping of R331X was assayed with PCR restriction fragment length polymorphism. PCR reactions were conducted in a reaction volume of 7.5 μL with 20 ng genomic DNA, 2× GC buffer, 200 μM dNTPs, 10 pmol of each primer and 1 unit of LA Taq polymerase (Takara, Tokyo, Japan). The PCR primers used were 5′-AGATGTCTGAAGGACCTTGGA-3′ as a forward primer and 5′-ACAGCTCAGAGGGACATGGA-3′ as a reverse primer. PCR was performed with 39 cycles of the following 94°C for 45 s, 54°C for 45 s and 74°C for 1 min in a thermocycler. Obtained PCR products showed a single fragment at 285 bp. Six μL of 285-bp product were then digested with 2 units of BspCNI restriction enzyme at 25 °C for 2 h. Digestion products were visualized on a 3 % agarose gel. Wild-type allele produced double band at 269 and 16 bp and mutant allele produced three bands at 165, 104 and 16 bp.

Table 1 C-peptide/insulin molar ratio in family members

Patient

OGTT (1) on admission

Time (min)	0	30	60	90	120
PG (mg/dL)	124	224	263	280	262
IRI (μU/mL)	65.7	114.8	191.5	279.1	290.1
CPR (ng/mL)	3.18	4.62	7.01	9.80	10.00
CPR/IRI molar ratio	2.21	1.84	1.67	1.60	1.57

OGTT (2) 2 weeks after admission

Time (min)	0	30	60	90	120
PG (mg/dL)	85	190	224	220	202
IRI (μU/mL)	52.7	136.9	187.4	239.2	313.6
CPR (ng/mL)	2.68	5.80	8.00	8.99	10.50
CPR/IRI molar ratio	2.32	1.93	1.95	1.72	1.53

Father

OGTT

Time (min)	0	30	60	90	120
PG (mg/dL)	88	169	256	214	172
IRI (μU/mL)	10.1	37.0	100.5	108.1	110.5
CPR (ng/mL)	1.24	3.14	6.96	8.05	8.22
CPR/IRI molar ratio	5.60	3.87	3.16	3.40	3.40

Grandmother

Fasting time	
PG (mg/dL)	146
IRI (μU/mL)	30.1
CPR (ng/mL)	2.51
CPR/IRI molar ratio	3.84

Results

An OGTT revealed a diabetic pattern with hyperinsulinemia (Table 1). The homeostasis model assessment of insulin resistance (HOMA-IR), an index of insulin resistance, was 20.1. The C-peptide/insulin molar ratio was extremely low. The fasting and 120 min levels were 2.21 and 1.57, respectively (normal level of fasting is 4.0<). An insulin tolerance test (0.1U/kg insulin i.v.) showed insulin resistance with only 37 % reduction in plasma glucose levels. Metformin was started from 250 mg/day and increased up to 500 mg/day. HbA1c levels improved to 5-6 % six months later. At that point in time, her fasting proinsulin level was 71.7 pmol/L when the IRI level was 49.1 μg/mL. Proinsulin/insulin molar ratio was 0.24 (normal 0.1-0.2). Her insulin levels were still high; however, the acanthosis nigricans had disappeared after she had regained diabetic control.

Her clinical course suggested two genetic diseases of glucose metabolism. One was the insulin gene mutation, as characterized by a low level C-peptide/insulin molar ratio, and sometimes presents as type 2 DM. The other was the insulin receptor gene mutation, which clinically demonstrated type A insulin resistance.

A sequencing analysis of the 22 exons as well as the intron-exon junctions identified a heterozygous mutation at nucleotide position 1072 substituting a termination codon for arginine 331, a conserved amino acid in the insulin-like growth factor I receptor and insulin receptor-related receptor, in the putative receptor L2 domain of the patient's insulin receptor (Fig. 1) [19]. No other mutations were found in any of the insulin receptor genes analyzed in this study.

Her father and grandmother also had the same

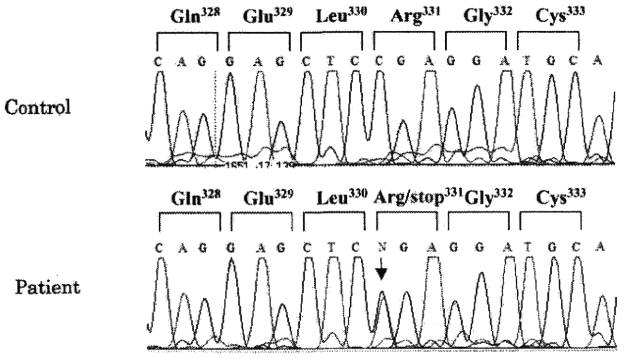

Fig. 1 Partial nucleotide sequence of the insulin receptor gene in the patient. Sequence from the patient is shown in comparison with that from the control. The patient is heterozygous for a mutation at the nucleotide position 1072, converting Arg 331(CGA) to a termination codon (TGA). An arrow indicates the position of mutation.

heterozygous mutation (data not shown). The fasting C-peptide/insulin molar ratio of her grandmother was relatively low under the treatment of sulfonylureas (3.84, IRI; 30.1 μU/mL, CPR 2.51 ng/mL). The HbA1c level of her father was 4.7 %, but OGTT showed impaired glucose tolerance (Table1). Although the fasting insulin level was 10.1 μU/mL, it increased up to 100 μU/mL in 60 -120 min. The C-peptide/insulin molar ratio was 5.60 in fasting and 3.40 in 120 min. They showed milder insulin resistance in comparison to the proband. The heterozygous mutation seemed to significantly affect the insulin resistance of the three subjects, even if no typical skin lesions were observed in either the father or grandmother.

One unrelated case of leprechaunism with R331X homozygous mutation was identified in Tokyo, Japan. The patient was born to unrelated parents at 39 weeks of gestation with a birth weight of 1743 g. She showed an extreme degree of insulin resistance (FPG, 200 mg/dL<; IRI 10,000 μU/mL<). She thereafter started to receive subcutaneous injections of recombinant human IGF-I. After treatment, her glucose metabolic abnormality was improved. Informed consent was obtained from her parents for sequence analysis. Her parents had R331X heterozygous mutation. They did not demonstrate any symptoms of diabetes mellitus. Information on the glucose tolerance including OGTT was unavailable.

These findings led to the hypothesis that insulin receptor genetic variants contribute to the variation of DM in the general population in Japan. An extensive search was done in 272 participants in a group medical examination that included 92 healthy cases of normoglycemia and 180 cases already diagnosed as type 2 DM or detected hyperglycemia. The search, however, failed to detect any R331X mutation in this local population.

Discussion

Type A insulin resistance was initially characterized in young female patients with acanthosis nigricans, ovarian hyperandrogenism and virilization [20]. Over 30 mutations have so far been described in these patients, which are mainly clustered in the tyrosine kinase domain of the insulin receptor [21, 22].

A nonsense mutation was identified in one allele of a patient substituting the termination codon (TGA) for the CGA codon normally encoding Arg^{331} located in a putative L2 domain, which is a single stranded right-hand beta-helix and is suggested to make up the bilobal ligand binding site [23]. The nonsense mutation at codon 331 truncated the C-terminal half of the receptor α subunit as well as the entire β subunit including the transmembrane anchor and the tyrosine kinase domain. Therefore, it is unlikely that this truncated receptor, translated from the mutant allele, would be either functional or located on the cell surface. In fact, extreme insulin resistance was observed in a female leprechaunism patient with homozygous R331X alleles.

Hyperinsulinemia is usually considered to be the result of resistance to the physiological effects of insulin and consequent compensatory increased insulin secretion. Recently, the C-peptide/insulin ratio is widely used as a surrogate of hepatic insulin clearance for the evaluation in type 2 DM or glucose intolerance [24, 25]. This index, should clarify whether impaired hepatic insulin clearance or increased insu-

lin secretion has a dominant effect on such patients. Insulin and C-peptide are secreted into the portal vein in a 1:1 molar ratio after β-cell stimulation by carbohydrate or other secretagogues. A large fraction of endogenous insulin is cleared by the liver, whereas C-peptide, which is cleared primarily by the kidney and has a lower metabolic clearance rate than insulin, and traverses the liver with essentially no extraction by hepatocytes [26, 27]. Diminished insulin clearance has been demonstrated to be an important underlying mechanism for the hyperinsulinemia found in various insulin-resistant conditions [28-30]. For example, to evaluate hyperinsulinemia in African Americans, at risk for type 2 DM, several studies used C-peptide/insulin molar ratio as an index of hepatic insulin clearance. African American children and adults showed lower C-peptide/insulin ratio than White Americans, thus suggesting that high insulin levels could be partly attributed to lower clearance [31, 32].

Therefore, the use of the C-peptide/insulin molar ratio reflects of hepatic insulin clearance [33]. A low C-peptide/insulin molar ratio of our patients suggests impaired hepatic insulin clearance because of, not only DM, but also abnormal insulin receptor expression in the liver. To this day, a low C-peptide/insulin molar ratio has not been substantially observed among individuals with type A insulin resistance. Two family cases with an insulin receptor gene mutation reported the presence of a low C-peptide/insulin molar ratio [34, 35]. They showed hyperinsulinemic hypoglycemia, severe insulin resistance and the C-peptide/insulin molar ratio ranged from 1.1 to 3.8.

As well as this reported cases, the molar ratio of the proband of our family was very low similar to that observed in subjects with insulin gene mutation. Previously, low C-peptide/insulin ratio was well reported to be a clinical feature of mutations in the human insulin gene causing either familial hyperinsulinemia or familial hyperproinsulinemia. The elevated circulating IRI consisted mainly of the unprocessed mutated proinsulin, which had accumulated because of proinsulin's relatively low clearance compared with insulin. In these subjects, proinsulin levels were tends to be extremely high, namely over three hundred pmol/L [36, 37]. Due to dramatic improvements in the assay techniques of IRI, cross-reactivity with proinsulin is normally seen at very low levels. Consequently, there have been no new reports regarding hyperproinsulinemia with insulin gene mutations for the last decade.

Recently, the fasting proinsulin/insulin ratio is used as a marker of β-cell dysfunction. In peripheral blood, fasting proinsulin accounts for 10-20% of insulin but it may reach values as high as 50 % in type 2 DM. Taura *et al.* evaluated the basal and dynamic proinsulin-insulin relationship to assess the β-cell function during OGTT in type 2 DM [38]. The proinsulin/insulin molar ratio was higher in type 2 DM (0.39 ± 0.05) subjects than normal (0.14 ± 0.01) and impaired glucose-tolerant (0.13 ± 0.02) subjects. In comparison to this study, the fasting proinsulin/insulin ratio of the proband, 0.20 was slightly higher than normal. It is difficult to consider that her low C-peptide/insulin molar ratio is derived from structural abnormalities in the proinsulin molecule.

We calculated the C-peptide/insulin molar ratio of several previous cases with insulin receptor gene mutation from data measured simultaneously. Severe cases, Rabson-Mendenhall syndrome or Donohue's syndrome, showed very low level (0.69 to 1.83) [14, 39-41]. Milder cases, type A insulin resistance or DM, also showed relatively low molar ratio (1.47 to 4.26) [35, 42]. However, most previous case reports only recorded the IRI data, more investigations are needed to discuss these clinical characteristics.

Interestingly, the patient's father did not show hyperinsulinemia while demonstrating a normal C-peptide/insulin molar ratio after fasting. However, after oral glucose ingestion, the insulin level increased 100.5 μU/mL/mL at 60 min and the molar ratio gradually decreased from 5.60 to 3.40. Meier *et al.* studied the C-peptide/insulin molar ratio as calculated at singular time points after oral glucose administration in non-diabetic subjects [37]. They reported that the molar ratio decreased to half level at 30 minutes and then it gradually increased up to the initial level through 120 min. In contrast to their data, the proband and her father showed a gradually decreasing pattern from 0 to 120 minutes. Receptor-mediated insulin endocytosis and degradation in hepatocyte underlie the basic mechanism of insulin clearance. Insulin is targeted for degradation after internalization, whereas the receptor recycles back to the cell surface [43]. CEACAM1, a transmembrane glycoprotein, plays a significant role in receptor-mediated insulin endocytosis [44]. *In vitro* studies suggest that upon its phosphorylation by the insulin receptor kinase, CEACAM1 binds indirectly to the receptor to undergo internalization in clathrin-coated vesicles as part of endocytosis complex [45].

CEACAM1 is considered to interact with two separate domains of the insulin receptor: a C-terminal for its phosphorylation, and cytoplasmic juxtamembrane domain required for internalization [46]. R331X mutant defects these important domains for endocytosis of insulin-insulin receptor complex. A reduction of endocytosis may also affect recycle of insulin receptor and may cause prolonged low hepatic extraction after glucose oral load observed in subjects having R331X mutation. Although her father showed normal data in fasting period, the oral glucose test may be a supplementary means for evaluating of insulin receptor mutant subjects.

As stated above, C-peptide is believed to be a better index of the pancreatic β-cell function than insulin because C-peptide levels are unaffected by hepatic clearance. When comparing the father's C-peptide levels of OGTT with proband, only a slight difference was observed. This result indicates that the insulin secreting function of β-cell is not substantially different and the cause of hyperinsulinemia in the proband is dominantly affected by impaired hepatic insulin clearance. The evaluation of the C-peptide/insulin molar ratio is thus considered to be a useful index for identifying genetic insulin resistance patients. On the other hand, a mild phenotype such as that observed in her father may not be effectively evaluated by the fasting data alone.

Unrelated Japanese patients with another mutation of the insulin receptor gene have been previously reported. They showed different phenotypes: one was detected as a heterozygous mutation in type A insulin resistance, while the other was detected as a compound heterozygous mutation in leprechaunism, thus indicating that the severity of such mutations will determine the phenotype [47]. The phenotype of heterozygous R331X differed substantially among the current family members. Although the proband and her grandmother showed diabetes mellitus with insulin resistance, the difference in the age of onset was around forty years. In addition, her father did not show insulin resistance after fasting. The reason for this difference may be conditioned by heredity and environment. The lifestyle for children has changed over the last few decades in Japan. The proband often consumed high caloric foods before detecting glucosuria. Numerous genetic factors related to diabetes mellitus have also been investigated. The insulin receptor pathway plays an important role in the glucose metabolism. The phenotype of a homozygous mutation, leprechaunism, revealed this important function in humans. However, a heterozygous mutation including Type A insulin resistance shows a mild phenotype. Variance in the current family case suggests that various genetic factors may therefore have played a role in their glucose metabolism. Contrary to expectations, the hypothesis that R331X determines the phenotype for glucose tolerance in Japanese people was ruled out. In addition, the influence of other reported mutations was unclear.

In conclusion, a nonsense mutation causing premature termination after amino acid 331 in the α subunit of the insulin receptor was identified in Japanese diabetes patients. The phenotype of R331X showed variety, and therefore further investigations, including determination of the mRNA level as well as ligand binding and receptor autophosphorylation, are thus called for to address the molecular mechanism by which this mutation leads to the occurrence of diabetes, as was observed in the current patient. In addition, the C-peptide/insulin molar ratio is considered to be a useful index for identifying genetic insulin resistance patients.

Acknowledgement

The study was supported in part by the Grants-in-Aid from the Japanese Ministry of Education, Culture, Sports, Science and Technology and the Global Center of Excellence (COE) program of Japan.

References

1. Massague J, Pilch PE, Czech MP (1980) Electrophoretic resolution of three major insulin receptor structures with unique subunit stoichiometries. *Proc Natl Acad Sci USA* 77: 7137-7141.
2. Kasuga M, Hedo JA, Yamada KM, Kahn CR (1982) The structure of insulin receptor and its subunits. Evidence for multiple nonreduced forms and a 210,000 possible proreceptor. *J Biol Chem 257*: 10392-10399.
3. Christiansen K, Tranum-Jensen J, Carlsen J, Vinten J (1991) A model for quaternary structure of human pla-

cental insulin receptor deduced from electron microscopy. *Proc Natl Acad Sci USA* 88: 249-252.
4. Ullrich A, Bell JR, Chen EY, Herrera R, Petruzzelli LM, TDull TJ, Gray A, Coussens L, Liao YC, Tsubokawa M, *et al.* (1985) Human insulin receptor and its relationship to tyrosine kinase family of oncogenes. *Nature* 313: 756-761.
5. Ebina Y, Ellis L, Jarnagin K, Edery M, Graf L, Clauser E, Ou JH, Masiarz F, Kan YW, Goldfine ID, *et al.* (1985) The human insulin receptor cDNA: the structural basis for hormone-activated transmembrane signaling. *Cell* 40: 747-758.
6. Kasuga M, Fujita-Yamaguchi Y, Blithe DL, Kahn CR (1983) Tyrosine-specific protein kinase activity is associated with the purified insulin receptor. *Proc Natl Acad Sci USA* 80: 2137-2141.
7. Rosen OM (1987) After insulin binds. *Science* 237: 1452-1458.
8. Taylor SI, Kadowaki T, Kadowaki H, Accili D, Cama A, McKeon C (1990) Mutations in insulin receptor gene in insulin-resistant patients. *Diabetes Care* 13: 257-279.
9. Taylor SI, Cama A, Accili D, Barbetti F, Quon MJ, de la Luz Sierra M, Suzuki Y, Koller E, Levy-Toledano R, Wertheimer E, *et al.* (1992) Mutation in the insulin receptor gene. *Endocri Rev* 13: 565-595.
10. Taylor SI (1992) Lessons from patients with mutation in the insulin-receptor gene. *Diabetes* 41: 1473-1490.
11. Taira M, Taira M, Hashimoto N, Shimada F, Suzuki Y, Kanatsuka A, Nakamura F, Ebina Y, Tatibana M, Makino H, *et al.* (1989) Human diabetes associated with a deletion of the tyrosine kinase domain of the insulin receptor. *Science* 245: 63-66.
12. Taylor SI, Accili D, Cama A, Kadowaki H, Kadowaki T, Imano E, Sierra ML (1991) Mutations in the insulin receptor gene in patients with genetic syndromes of insulin resistance. *Adv Exp Med Biol* 293: 197-213.
13. Longo N, Langley SD, Griffin LD, Elsas LJ (1992) Reduced mRNA and a nonsense mutation in the insulin receptor gene produce heritable severe insulin resistance. *Am J Hum Genet* 50: 998-1007.
14. Longo N, Wang Y, Smith SA, Langley SD, DiMeglio LA, Giannella-Neto D (2002) Genotype-phenotype correlation in inherited severe insulin resistance. *Hum Mol Genet* 11: 1465-1475.
15. Longo N, Singh R, Griffin LD, Langley SD, Parks JS, Elsas LJ (1994) Impaired growth in Rabson-Mendenhall syndrome: Lack of effect of growth hormone and insulin-like growth factor I. *J Clin Endocrinol Metab* 79: 799-805.
16. Kahn CR, Flier JS, Bar RS, Archer JA, Gorden P, Martin MM, Roth J (1976) The syndromes of insulin resistance and acanthosis nigricans. Insulin-receptor disorders in man. *N Eng J Med* 294: 739-745.
17. Bell GI, Picter RL, Rutter WJ, Cordell B, Tischer E, Goodman HM (1980) Sequence of the human insulin gene. *Nature* 284: 26-32.
18. Barbetti F, Gejiman PV, Taylor SI, Raben N, Cama A, Bonora E, Pizzo P, Moghetti P, Muggeo M, Roth J (1992) Detection of mutations in insulin receptor gene by denaturing gradient gel electrophoresis. *Diabetes* 41: 408-415.
19. Shier P, Watt VM (1983) Primary structure of a putative receptor for a ligand of the insulin family. *J Biol Chem* 264: 359-399.
20. Tritos NA, Mantzoros CS (1998) Syndromes of severe insulin resistance. *J Clin Endocr Metab* 83: 3025-3030.
21. Kadowaki H, Kadowaki T, Cama A, Marcus-Samuel B, Rovira A, Bevins CL, Taylor SI (1990) Mutagenesis of Lysine 460 in the human insulin receptor. *J Biol Chem* 265: 21285-21296.
22. Moller DE, Yokota A, White MF, Pazianos AG, Flier JS (1990) A naturally occurring mutation of insulin receptor alanine 1134 impaires tyrosine kinase function and is associated with dominantly inherited insulin resistance. *J Biol Chem* 265: 14979-14985.
23. Garrett TPJ, McKern NM, Lou M, Frenkel MJ, Bentley JD, Lovrecz GO, Elleman TC, Cosgrove LJ, Ward CW (1998) Crystal structure of the first three domains of the type-1 insulin-like growth factor receptor. *Nature* 394: 395-399.
24. Meier JJ, Holst JJ, Schmid WE, Nauck MA (2007) Reduction of hepatic insulin clearance after oral glucose ingestion is not mediated by glucagon-like peptide 1 or gastric inhibitory polypeptide in humans. *Am J Physiol Endocrinol Metab* 293: E846-E856.
25. Osei K, Rhinesmith S, Gaillard T, Schuster D (2003) Metabolic effects of chronic glipizide gastrointestinal therapeutic system on serum glucose, insulin secretion, insulin sensitivity, and hepatic insulin extraction in glucose-tolerant, first degree relatives of African American patients with type 2 diabetes: new insights on mechanisms of action. *Metabolism* 52: 565-572.
26. Horwitz DL, Starr JI, Mako ME, Blackard WG, Rubenstein AH (1975) Proinsulin, insulin, and C-peptide concentrations in human portal and peripheral blood. *J Clin Invest* 55: 1278-1283.
27. Shapiro ET, Tillil H, Miller MA, Frank BH, Galloway JA, Rubenstein AH, Polonsky KS (1987) Insulin secretion and clearance. Comparison after oral and intravenous glucose. *Diabetes* 36: 1365-1371.
28. Polonsky KS, Given BD, Hirsch L, Shapiro ET, Tillil H, Beebe C, Galloway JA, Frank BH, Karrison T, Van Ceuter E (1988) Quantitative study of insulin secretion and clearance in normal and obese subjects. *J Clin Invest* 81: 435-441.
29. Jones CNO, Pei D, Staris P, Polonsky KS, Ida Chen YD, Reaven GM (1997) Alternations in the glucose-stimulated insulin secretory dose-response curve and in insulin clearance in nondiabetic insulin-resistant indi-

viduals. *J Clin Endocrinol Metab* 82: 1834-1838.
30. Inokuchi T, Watanabe K, Kameyama H, Orita M (1988) Altered basal C-peptide/insulin molar ratio in obese patients with fatty liver. *Jpn J Med* 27: 272-276.
31. Arslanian SA, Saad R, Lewy V, Danadian K, Janosky J (2002) Hyperinsulinemia in African-American Children. *Diabetes* 51: 3014-3019.
32. Osei K, Schster DP, Owusu SK, Amoah AG (1996) Race and ethnicity determine serum insulin and C-peptide concentrations and hepatic insulin extraction and insulin clearance: comparative studies of three populations of West African ancestry and white Americans. *Metabolism* 46: 53-58.
33. Polonsky KS, Rubenstein AH (1984) C-peptide as a measure of the secretion and hepatic extraction of the insulin. Pitfalls and limitations. *Diabetes* 33: 486-494.
34. Højlund K, Hansen T, Lajer M, Henriksen JE, Levin K, Lindholm J, Pedersen O, Beck-Nielsen H (2004) A novel syndrome of autosomal-dominant hyperinsulinemic hypoglycemia linked to a mutation in the human insulin receptor gene. *Diabetes* 53: 1592-1598.
35. Huang Z, Li Y, Tang T, Xu W, Liao Z, Yao B, Hu G, Weng J (2009) Hyperinsulinaemic hypoglycemia associated with a heterozygous missense mutation of R1174W in the insulin receptor (IR) gene. *Clin Endocrinol* 71: 659-665.
36. Røder ME, Vissing H, Nauck MA (1996) Hyperproinsulinemia in a three-generation Caucasian family due to mutant proinsulin (Arg65→His) not associated with impaired glucose tolerance: the contribution of mutant proinsulin to insulin bioactivity. *J Clin Endocrinol Metab* 81: 1634-1640.
37. Meier JJ, Gallwitz B, Siepmann N, Holst JJ, Deacon CF, Schmidt WE, Nauck MA (2003) The reduction in hepatic insulin clearance after oral glucose is not mediated by gastoric inhibitory polypeptide (GIP). *Regul Pept* 113: 95-100.
38. Taura A, Pacini G, Kautzky-Willer A, Ludvik B, Prager R, Thomaseth K (2003) Basal and dynamic proinsulin-insulin relationship to assess β-cell function during OGTT in metabolic disorders. *Am J Physiol Endocrinol Metab* 285: E155-E162.
39. Thiel CT, Knebel B, Knerr I, Sticht H, Müller-Wieland D, Zenker M, Reis Andre, Dörr HG, Rauch A (2008) Two novel mutations in the insulin binding impairment in a patient with Rabson-Mendenhall syndrome. *Mol Genet and Metab* 94: 356-362.
40. Unal S, Aycan Z, Halsall DJ, Kibar AE, Eker S, Ozaydin E (2009) Donohue syndrome in a neonate with homozygous deletion of exon 3 of the insulin receptor gene. *J Pediatr Endocrinol Metab* 22: 669-674.
41. Tuthill A, Semple RK, Day R, Soos MA, Sweeney E, Seymour PJ, Didi M, O'Ragilly S (2007) Functional characterization of a novel insulin receptor mutation contributing to Rabson-Mendenhall syndrome. *Clin Endocrinology* 66: 21-26.
42. Riqué S, Nogués C, Ibáñez L, Marcos MV, Ferragut J, Carrascosa A, Potau N (2000) Identification of three novel mutations in the insulin receptor gene in type A insulin resistant patients. *Clin Genet* 57: 67-69.
43. Carpentier JL (1993) Robert Feulgen Prize Lecture 1993. The journey of the insulin receptor into the cell: from cellular biology to pathophysiology. *Histochemistry* 100: 169-184.
44. Poy MN, Yang Y, Rezaei K, Fernström MA, Lee AD, Kido Y, Erickson SK, Najjar SM (2002) *Nature Genet* 30: 270-276.
45. Choice CV, Howard MJ, Poy MN, Hankin MH, Najjar SM (1998) *J Biol Chem* 273: 22194-22200.
46. Najjar SN (2002) Regulation of insulin action by CEACAM1. *Trends Endocrinol Metab* 13: 240-245.
47. Kadowaki H, Takahashi Y, Ando A, Momomura K, Kaburagi Y, Quin JD, MacCuish AC, Koda N, Fukushima Y, Taylor SI, Akanuma Y, Yazaki Y, Kadowaki T (1997) Four mutant alleles of the insulin receptor gene associated with genetic syndromes of extreme insulin resistance. *Biochem. Biophys. Res. Commun* 237: 516-520.

THE JOURNAL OF BIOLOGICAL CHEMISTRY VOL. 285, NO. 9, pp. 6693–6705, February 26, 2010

Spontaneous Development of Endoplasmic Reticulum Stress That Can Lead to Diabetes Mellitus Is Associated with Higher Calcium-independent Phospholipase A_2 Expression

*A ROLE FOR REGULATION BY SREBP-1**

Received for publication, November 11, 2009, and in revised form, December 18, 2009 Published, JBC Papers in Press, December 23, 2009, DOI 10.1074/jbc.M109.084293

Xiaoyong Lei[‡], Sheng Zhang[‡], Suzanne E. Barbour[§], Alan Bohrer[‡], Eric L. Ford[‡], Akio Koizumi[¶], Feroz R. Papa[‖], and Sasanka Ramanadham[‡1]

From the [‡]Department of Medicine, Mass Spectrometry Resource, and Division of Endocrinology, Metabolism, and Lipid Research, Washington University School of Medicine, St. Louis, Missouri 63110, the [§]Department of Biochemistry and Molecular Biology, Virginia Commonwealth University School of Medicine, Richmond, Virginia 23298, the [¶]Department of Health and Environmental Sciences, Kyoto Graduate School of Medicine, Kyoto 606-8501, Japan, and the [‖]California Institute for Quantitative Biosciences, University of California, San Francisco, California 94143

Our recent studies indicate that endoplasmic reticulum (ER) stress causes INS-1 cell apoptosis by a Ca^{2+}-independent phospholipase A_2 ($iPLA_2\beta$)-mediated mechanism that promotes ceramide generation via sphingomyelin hydrolysis and subsequent activation of the intrinsic pathway. To elucidate the association between $iPLA_2\beta$ and ER stress, we compared β-cell lines generated from wild type (WT) and Akita mice. The Akita mouse is a spontaneous model of ER stress that develops hyperglycemia/diabetes due to ER stress-induced β-cell apoptosis. Consistent with a predisposition to developing ER stress, basal phosphorylated PERK and activated caspase-3 are higher in the Akita cells than WT cells. Interestingly, basal $iPLA_2\beta$, mature SREBP-1 (mSREBP-1), phosphorylated Akt, and neutral sphingomyelinase (NSMase) are higher, relative abundances of sphingomyelins are lower, and mitochondrial membrane potential ($\Delta\Psi$) is compromised in Akita cells, in comparison with WT cells. Exposure to thapsigargin accelerates $\Delta\Psi$ loss and apoptosis of Akita cells and is associated with increases in $iPLA_2\beta$, mSREBP-1, and NSMase in both WT and Akita cells. Transfection of Akita cells with $iPLA_2\beta$ small interfering RNA, however, suppresses NSMase message, $\Delta\Psi$ loss, and apoptosis. The $iPLA_2\beta$ gene contains a sterol-regulatory element, and transfection with a dominant negative SREBP-1 reduces basal mSREBP-1 and $iPLA_2\beta$ in the Akita cells and suppresses increases in mSREBP-1 and $iPLA_2\beta$ due to thapsigargin. These findings suggest that ER stress leads to generation of mSREBP-1, which can bind to the sterol-regulatory element in the $iPLA_2\beta$ gene to promote its transcription. Consistent with this, SREBP-1, $iPLA_2\beta$, and NSMase messages in Akita mouse islets are higher than in WT islets.

β-Cell loss due to apoptosis contributes to the progression and development of Type 1 or Type 2 diabetes mellitus (T1DM[2] or T2DM, respectively). This is supported by autopsy studies that reveal reduced β-cell mass in obese T2DM subjects in comparison with obese non-diabetic subjects (1, 2) and reveal that the loss in β-cell function in non-obese T2DM is associated with decreases in β-cell mass (3, 4). Other evidence suggests that cytokines cause β-cell apoptosis during the development of autoimmune T1DM (5–8). It is therefore important to understand the mechanisms underlying β-cell apoptosis if this process is to be prevented or delayed.

β-Cell mass is regulated by a balance between β-cell replication/neogenesis and β-cell death resulting from apoptosis (9, 10). Findings in rodent models of T2DM (10, 11) and in human T2DM (3, 4) indicate that the decrease in β-cell mass in T2DM is not attributable to reduced β-cell proliferation or neogenesis but to increased β-cell apoptosis (12). In addition to the intrinsic and extrinsic apoptotic pathways, apoptosis due to prolonged endoplasmic reticulum (ER) stress (12, 13) has been reported in various diseases, including Alzheimer and Parkinson diseases (14).

Evidence from the Akita (15, 16) and NOD.k iHEL (17) mouse models suggests that ER stress can also lead to the development of diabetes mellitus as a consequence of β-cell apoptosis. Further, mutations in genes encoding the ER stress-transducing enzyme pancreatic ER kinase (PERK) (18) and the ER-resident protein involved in degradation of malfolded ER proteins have been clinically linked to diminished β-cell health (19, 20). Other reports suggest that ER stress may also play a

* This work was supported, in whole or in part, by National Institutes of Health Grants R01-DK69455, P41-RR00954, P60-DK20579, P30-DK56341, and DK065671. This work was also supported by a grant from the American Diabetes Association (to S. R.) and National Science Foundation Grant NSF-MCB-0544068 (to S. E. B.).

[1] To whom correspondence should be addressed: Dept. of Medicine, Washington University School of Medicine, Campus Box 8127, 660 S. Euclid Ave., St. Louis, MO 63110. Tel.: 314-362-8194; Fax: 314-362-7641; E-mail: sramanad@dom.wustl.edu.

[2] The abbreviations used are: T1DM, Type 1 diabetes mellitus; T2DM, Type 2 diabetes mellitus; AK, Akita; pAkt, phosphorylated Akt; PERK, pancreatic ER kinase; pPERK, phosphorylated PERK; BEL, bromoenol lactone suicide inhibitor of $iPLA_2\beta$; DN, dominant negative; ER, endoplasmic reticulum; ESI/MS/MS, electrospray ionization/tandem mass spectrometry; GPC, glycerophosphocholine; $iPLA_2\beta$, β-isoform of group VIA Ca^{2+}-independent phospholipase A_2; NSMase, neutral sphingomyelinase; PBS, phosphate-buffered saline; PLA_2, phospholipase A_2; mSREBP-1, mature (or processed) SREBP-1; TUNEL, terminal deoxynucleotidyl transferase-mediated (fluorescein) dUTP nick end labeling; WT, wild type; siRNA, small interfering RNA; DAPI, 4′,6-diamidino-2-phenylindole; qRT-PCR, quantitative reverse transcription-PCR; SRE, sterol-regulatory element; $DiOC_6(3)$, 3,3′-dihexyloxacarbocyanine iodide.

prominent role in the autoimmune destruction of β-cells during the development of T1DM (6, 21, 22). Because the secretory function of β-cells endows them with a highly developed ER and the β-cell is one of the cells most sensitive to nitric oxide (23), it is not unexpected that β-cells exhibit a heightened susceptibility to autoimmune-mediated ER stress (24, 25). In support of this, Wolfram syndrome, which is associated with juvenile onset diabetes mellitus, is recognized to be a consequence of chronic ER stress in pancreatic β-cells (21, 26).

In view of the evidence suggesting that ER stress-induced β-cell apoptosis may be a factor in the development of diabetes mellitus, it was of interest to elucidate the mechanisms involved. Recent work from our laboratory led to the identification of a Ca^{2+}-independent phospholipase A_2 (iPLA$_2$β) as a key participant in ER stress-mediated apoptosis of INS-1 insulinoma cells. The iPLA$_2$β, classified as a Group VIA isoform of iPLA$_2$, is a member of a large family of PLA$_2$s (27) that is cytosolic and does not require Ca^{2+} for activity (28–30). It is activated by ATP, is inhibited by the bromoenol lactone suicide substrate (BEL) inhibitor of iPLA$_2$β (31), and is recognized to have a role in signal transduction (28, 31–39). We found that induction of ER stress with the sarcoendoplasmic reticulum Ca^{2+}-ATPase inhibitor thapsigargin causes INS-1 cell apoptosis that is amplified by overexpression of iPLA$_2$β and is inhibited by BEL (40).

Further work indicated that ER stress activates iPLA$_2$β in INS-1 cells, leading to neutral sphingomyelinase (NSMase) induction and generation of ceramides via hydrolysis of sphingomyelins (41). Subsequently, the ceramides trigger mitochondrial apoptotic processes and cell death ensues. Consistent with this proposed mechanism, inhibition of iPLA$_2$β or NSMase suppresses sphingomyelin hydrolysis and ceramide generation, mitochondrial abnormalities, and apoptosis (42).

Although a link between iPLA$_2$β and ER stress-induced apoptotic pathway was gleaned from the above observations, it was derived from studies in which a chemical agent was used to induce ER stress and iPLA$_2$β expression levels were genetically manipulated in an insulinoma cell line. Of importance was to determine whether a similar link existed under conditions where ER stress developed in the β-cell in the absence of chemical intervention. Here, we present studies in a β-cell line established from Akita mice (43), which contain a spontaneous mutation of the insulin 2 gene (*Ins2*) (C96Y) that results in misfolding insulin in the ER leading to development of hyperglycemia/diabetes due to ER stress-induced β-cell apoptosis (44, 45). Our findings reveal for the first time that predisposition to ER stress is associated with increased expression of iPLA$_2$β and that its expression is modulated by activation of SREBP-1 (sterol-regulatory element-binding protein-1). We also present the first evidence in Akita mouse islet β-cells that substantiates these findings.

EXPERIMENTAL PROCEDURES

Materials—The sources for the material used were as follows: 16:0/[^{14}C]18:2-GPC (55 mCi/mmol), rainbow molecular mass standards, and ECL reagent (Amersham Biosciences); low melting agarose (Applied Biosystems Inc., Foster City, CA); Coomassie reagent, SDS-PAGE supplies, and Triton X-100 (Bio-Rad); mitochondrial membrane potential detection kit (Cell Tech. Inc., Mountain View, CA); paraformaldehyde (Electron Microscopy Sciences, Ft. Washington, PA); xylene (Fisher); secondary antibody goat anti-rabbit IgG Alexa Fluor 594 (Invitrogen); secondary antibody Cy3-affinipure bovine anti-goat IgG(H + L) (Jackson ImmunoResearch Laboratories Inc., West Grove, PA); DiOC$_6$(3) and Hoechst dye and Slow Fade® light antifade kit (Molecular Probes, Inc., Eugene, OR); peroxidase-conjugated goat anti-rabbit IgG antibody, TUNEL kit (Roche Applied Science); Lipofectamine 2000 (Invitrogen); siRNA kit (Qiagen, Valencia, CA); primary antibodies (Santa Cruz Biotechnology, Inc., Santa Cruz, CA); agarose, collagenase, protease inhibitor mixture, thapsigargin, common reagents, and salts (Sigma); tissue marking dye (Triangle Biomedical Sciences Inc. (Durham, NC) and Vector Laboratories, Inc. (Burlingame, CA).

Cell Culture and Treatment—The Akita and wild type (WT) cells were generated as follows. A transgenic mouse line that harbored the modified human insulin promoter connected to the SV40 T antigen coding region on C57BL/6 mice (IT3 line) was kindly provided by Dr. Jun-Ichi Miyazaki (46). Male offspring were mated with female Akita mice (*Ins2*$^{+/AK}$) (45) on a C57BL/6 background. Insulinomas that developed in the pancreas of the progeny were removed and cultured in Dulbecco's modified Eagle's medium containing high glucose and 15% fetal bovine serum (43). Pancreatic β-cell lines were established from the cells grown as monolayers on culture dishes. Several cell lines were obtained for *Ins2*$^{+/AK}$ and for wild type *Ins2*$^{+/+}$.

The cells were cultured in Dulbecco's modified Eagle's medium (containing 10 μl of β-mercaptoethanol/200 ml) as described (43). The medium was exchanged every 2 days, and the cells were split, as required, once a week. Cells (~25–30 passages) were grown to 80% confluence in cell culture dishes and harvested following treatment with vehicle (DMSO, 0.50 μl/ml) or thapsigargin (0.5 μM). The cells were harvested at various times (2–16 h) and prepared for various analyses described below. All incubations were done at 37 °C under an atmosphere of 95% air, 5% CO_2.

In Situ Detection of DNA Cleavage by TUNEL and DAPI Staining—Cells were harvested and washed twice with ice-cold PBS and then immobilized on slides by cytospin (40) and fixed with 4% paraformaldehyde (in PBS, pH 7.4, 1 h, room temperature). The cells were then processed for TUNEL staining analyses as described (42). Incidence of apoptosis was assessed under a fluorescence microscope (Nikon Eclipse TE300) using a fluorescein isothiocyanate filter. Cells with TUNEL-positive nuclei were considered apoptotic. DAPI staining was used to determine the total number of cells in a field. A minimum of three fields per slide was used to calculate the percentage of apoptotic cells.

Assessment of Mitochondrial Membrane Potential (ΔΨ)—Loss of ΔΨ is an important step in the induction of cellular apoptosis (47). Akita and WT cell ΔΨ was initially measured using a commercial kit by flow cytometry (BD Biosciences) as described (42). Fluorescence in cells was monitored at an excitation wavelength of 488 nm. Although these analyses yield quantitative results, they were hampered by the tendency of these cells to clump together, causing the fluorescence peaks to

be broad. To address this issue, a second method to monitor $\Delta\Psi$ was established. Cells were plated in a 6-well plate with the coverslips and cultured up to semiconfluence. After washing with PBS twice at room temperature, the coverslips were incubated with $DiOC_6(3)$ solution (175 nM) for 15 min under an atmosphere of 5% CO_2, 95% air (37 °C). The Hoechst reagent (5 μg/ml) was then added to stain the nucleus. After 20 min, the coverslips were rinsed with PBS, mounted on slides, and the cells were immediately examined using a confocal laser-scanning microscope (Zeiss) with a 488-nm argon laser and a 405-nm diode laser.

Immunoblotting Analyses—Cells were harvested and sonicated, and an aliquot (30 μg) of lysate protein was analyzed by SDS-PAGE (8 or 15%), transferred onto Immobilon-P polyvinylidene difluoride membranes, and processed for immunoblotting analyses as described (40). The targeted factors and the primary antibody concentrations were as follows: phosphorylated PERK (pPERK) (1:1000), iPLA$_2$β (T-14) (1:500), caspase-3 (1:1000), SREBP-1 (1:1000), pAkt (1:1000), and tubulin (1:2000). The secondary antibody concentration was 1:10,000. Immunoreactive bands were visualized by ECL.

Assay for iPLA$_2$β Activity—Cytosol fraction was prepared from Akita and WT cells and harvested, and protein concentration was determined using Coomassie reagent. Ca^{2+}-independent PLA_2 catalytic activity in an aliquot of cytosolic protein (30 μg) was assayed under zero Ca^{2+} conditions (no added Ca^{2+} plus 10 mM EGTA) in the presence of 16:0/[^{14}C]18:2-GPC (5 μM) as the substrate, and specific enzymatic activity was quantitated as described (40). To verify that the phospholipase activity is manifested by iPLA$_2$β, activity was also assayed in the presence of ATP (10 mM) or BEL (1 μM).

Sphingomyelin Analyses by ESI/MS/MS—Sphingomyelins are formed by reaction of a ceramide with CDP-choline, and similar to GPC lipids, they contain a phosphocholine as the polar headgroup. This feature of sphingomyelins facilitates identification of sphingomyelin molecular species by constant neutral loss scanning of trimethylamine ($[M + H]^+ - N(CH_3)_3$) or constant neutral loss of 59 as described (41). The prominent ions in the total ion current spectrum are those of the even mass PC molecular species, and these mask the odd mass sphingomyelin signals (41). Constant neutral loss of 59, however, facilitates emergence of signals for sphingomyelin species at odd *m/z* values, reflecting loss of nitrogen. Lipid extracts were prepared as above in the presence of a 14:0/14:0-GPC (*m/z* 684, 8 μg) internal standard, which is not an endogenous component of β-cell lipids, and analyzed by ESI/MS/MS. Sphingomyelins content in the samples was determined based on standard curves generated using commercially available brain and egg sphingomyelins with a known percentage of each fatty acid constituent and 14:0/14:0-GPC (*m/z* 684, 8 μg) as an internal standard as described (41). Total (pmol) sphingomyelin species in each fraction was determined and normalized to total phosphate (μmol of PO_4).

Transient Transfection of Dominant Negative (DN) SREBP-1—A DN SREBP-1 vector (Addgene plasmid 8885) was obtained from Addgene (Cambridge, MA). The plasmid developed by Kim and Spiegelman (49) expresses truncated ADD1 with a tyrosine to alanine mutation at amino acid 320. WT and Akita cells were cultured as described above and transfected 1 day before 90–95% confluence using Lipofectamine 2000 (Invitrogen). Briefly, DN SREBP-1 was diluted in 50 μl of Opti-MEM I reduced serum medium and mixed gently. After a 5-min incubation, DN SREBP-1 was mixed with diluted Lipofectamine 2000 (total volume, 100 μl). The mixture was incubated for 20 min at room temperature and used to transfect WT and Akita cells cultured in a 6-well plate. The cells were incubated at 37 °C under an atmosphere of 95% air, 5% CO_2 for 48 h prior to experimentation.

Suppression of iPLA$_2$β Expression—To knock down iPLA$_2$β, wild type and Akita cells were transfected with iPLA$_2$β siRNA according to the manufacturer's instructions (Qiagen, Valencia, CA). Cells were seeded in wells with culture medium containing serum and antibiotics and allowed to reach 50–80% confluence. The cells were then transfected with either control siRNA (*si** in Fig. 7) or iPLA$_2$β siRNA (*si* in Fig. 7). The siRNAs were prepared in dilution buffer and mixed gently with RNAiFect transfection reagent. The mixture was then incubated at room temperature for 10–15 min to allow formation of transfection complexes. The complexes were then gently added to the cells. The cells were cultured with the transfection complexes at 37 °C under an atmosphere of 95% air, 5% CO_2 for 72 h prior to experimentation.

Islet Isolation—Male mice (4–5 weeks of age) were anesthetized with ketamine/xlyazine mixture (0.75 μl/g body weight) prior to euthanization by cervical dislocation. The abdomen was isolated, and pancreata were isolated as described (50). The common bile duct was clamped at the duodenum-bile duct junction, and collagenase/Krebs-Ringer buffer (5 ml) was injected into the pancreas via the duct. Once the pancreas was completely distended, it was removed and placed in a scintillation vial with collagenase/Krebs-Ringer buffer (2.5 ml) and incubated in a 37 °C water bath for 13 min. The vial was then vigorously shaken for 90 s, followed by washing (three times) of the pancreas with Krebs-Ringer buffer containing 1 mM $CaCl_2$ (50 ml). The pancreas was then resuspended in incomplete RPMI 1640 (without FBS or penicillin/streptomycin, 25 ml) and poured through a 70-μm cell strainer into a Petri dish. The cells were washed further with incomplete RPMI 1640 (75 ml). The cell strainer was then inverted and rinsed with complete RPMI 1640 (10% fetal bovine serum, 2× penicillin/streptomycin, 25 ml) to collect the remaining islets in solution. The islets were then hand-picked under a microscope, counted, and incubated overnight in media under an atmosphere of 5% CO_2, 95% and 37 °C. Typical islet yields ranged from 25 to 50 from the Akita mice and 150 from WT mice. The islets were used to prepare total RNA for message and for immunostaining analyses, as described below.

Quantitative Reverse Transcription-PCR (qRT-PCR)—Total RNA was prepared from cells and islets cells using the RNeasy kit (Qiagen Inc.) as described (41, 42). cDNA was then generated using the SuperScriptII kit (Invitrogen) and heat-inactivated (70 °C for 15 min). PCR amplifications were performed using the SYBR Green PCR kit in an ABI 7000 detection system (Applied Biosystems). The primers were designed based on known mouse sequences for iPLA$_2$β, SREBP-1, NSMase, and control 18 S provided in the GenBank™ data base with identi-

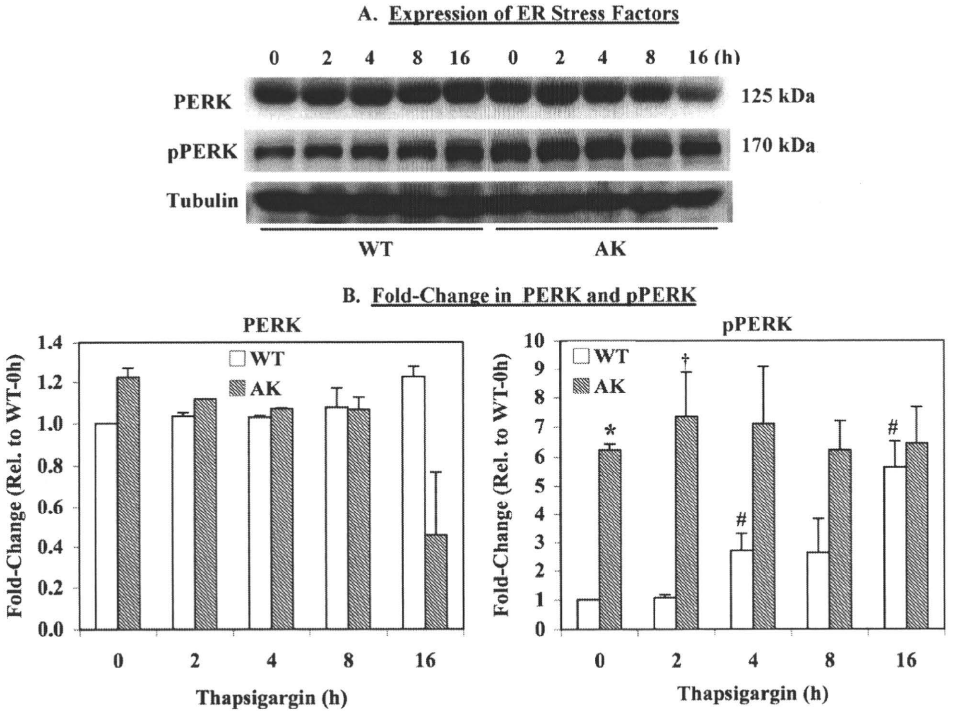

FIGURE 1. **Basal expression of ER stress factors and apoptotic factors.** WT and AK β-cells were harvested at various times after exposure to thapsigargin (0.50 μM), and 30 μg of lysate protein was processed for immunoblotting analyses for PERK and pPERK. Tubulin was used as a loading control. These analyses were done three separate times. *A*, immunoblot. A representative blot for PERK and pPERK is presented. *B*, densitometry. The ratios of PERK- and pPERK-immunoreactive bands to the corresponding tubulin band were determined, and means ± S.E. of -fold change relative to WT at 0 h are presented. * and †, significantly different from corresponding WT, $p < 0.001$ and $p < 0.05$, respectively. #, significantly different from WT at 0 h, $p < 0.05$.

fication numbers 53357, 20787, 20598, and 19791, respectively. The sense/antisense primer sets were as follows: iPLA$_2$β, gcccctggccattctacacagta/cacctcatccttcatacggaagt; SREBP-1, ccagaggtgagcctgacaa/agcctctgcaatttccagatct; NSMase, ctgagtacagccgacagaagga/gggccagttcccaagctt; 18 S, gccgctagaggtgaaattcttg/cattcttggcaaatgctttcg.

Immunostaining—Islets were fixed in 10% formalin and 5 μl of tissue marking dye, followed by the addition of 150 μl of low melting agarose. The mixture was spun down quickly to settle the islets at one surface of the agarose, which was then allowed to solidify. The islet-containing blocks were then processed, and paraffin sections (8–10 μm) were prepared for staining for iPLA$_2$β and SREBP-1. The sections were incubated overnight with primary antibodies (1:25), washed with PBS (4 × 30 min), incubated for 2–3 h with secondary antibodies (1:100 of Cy3 for iPLA$_2$β and Alexa Fluor 594 for SREBP-1), and washed with PBS (three times for 10 min each). DAPI stain (20–30 μl) was then added, and the sections were sealed with a coverslip using nail polish.

Statistical Analyses—Data were converted to mean ± S.E. values, and Student's *t* test was applied to determine significant differences between two samples ($p < 0.05$). The *n* value for each analysis is indicted in the figure legends.

RESULTS

Expression of ER Stress Factors in Akita β-Cells—As part of the unfolded protein response, various ER factors are induced to alleviate ER stress. One such marker of unfolded protein response activation is pPERK (51). Because the Akita β-cells are reported to be a spontaneous model of ER stress, we compared pPERK levels in these cells with those in WT β-cells. As shown in Fig. 1, basal pPERK is greater in the Akita relative to wild type cells. Although exposure to thapsigargin induced pPERK expression in both the WT and Akita cells, they peaked earlier and remained higher in the Akita cells (Fig. 1*B*). These observations are consistent with the original findings of increased ER molecular chaperones and ER stress response element-binding transcription factors in the Akita cells (43) and confirm that the Akita cells are predisposed to developing ER stress and that they are a good model for the study of underlying mechanisms that contribute to β-cell apoptosis due to ER stress.

Reduced Sphingomyelins in Akita β-Cells—We reported that ER stress-induced ceramide generation via NSMase-catalyzed sphingomyelin hydrolysis was a critical contributor to INS-1 cell apoptosis (41, 42). If this pathway is activated by ER stress, this should be reflected by reduced abundances of sphingomyelin molecular species in the Akita cells. To examine this possibility, WT and Akita cells were harvested under basal conditions and analyzed by ESI/MS/MS. The spectra in Fig. 2 display tracings of Li^+ adducts of sphingomyelin species in cell lysates after the addition of the 14:0/14:0-GPC internal standard, which is represented in the spectrum by its $(M + Li^+)^+$ ion (*m/z* 684). Similar to the INS-1 cells, the major sphingomyelin species endogenous to WT and Akita β-cells are 16:0 (*m/z* 709), 18:0 (*m/z* 737), 22:0 (*m/z* 693), 24:1 (*m/z* 819), and 24:0 (*m/z* 821). The spectra were acquired by monitoring constant neutral loss of 59, as described (52), in WT (Fig. 2*A*) and Akita (Fig. 2*B*) cells. As reflected by the decreases in the intensity of ions representing them, the relative abundances of the sphingomyelin molecular species are decreased in the Akita cells in comparison with WT cells. Normalization of individual sphingomyelin molecular species to lipid phosphorus revealed the 16:0, 18:0, 22:0, 24:0, and 24:1 species in the Akita cells to be 47 ± 9, 22 ± 2, 75 ± 4, 95 ± 4, and 78 ± 10% of WT cells, respectively. The total pool of sphingomyelins (pmol/μmol of PO_4) revealed a 48% decrease in sphingomyelin abundance in the Akita cells, relative to the WT cells (Fig. 2*C*). These findings indicate that hydrolysis of sphingomyelins is ramped up in the Akita cells and suggest the possibility of consequential triggering of mitochondrial abnormalities.

Compromised ΔΨ in Akita β-Cells—Loss of ΔΨ is an important step in the induction of cellular apoptosis (47). Because thapsigargin-induced ER stress caused a loss in INS-1 cell ΔΨ

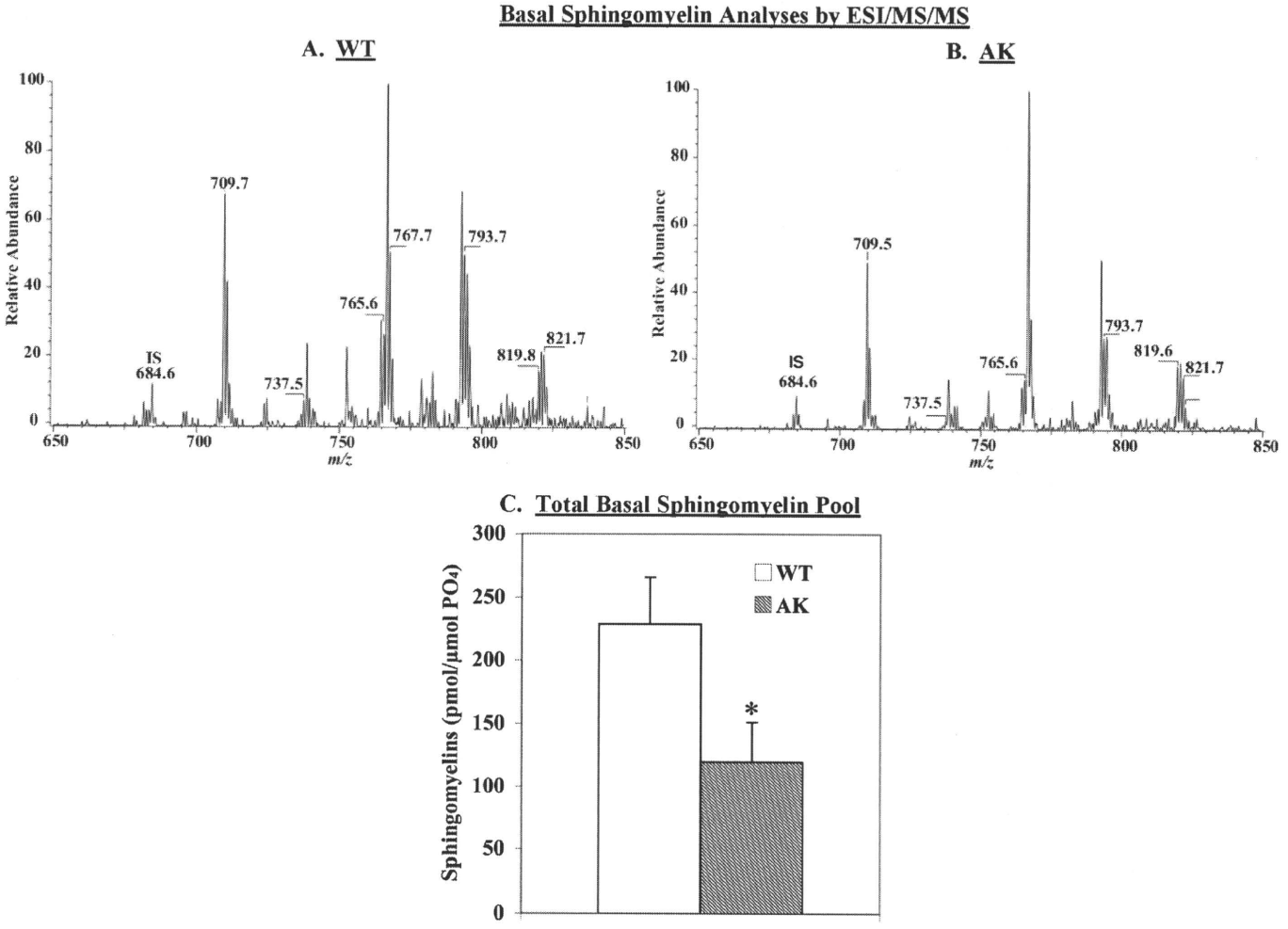

FIGURE 2. **Sphingomyelin analyses by ESI/MS/MS.** Phospholipids were extracted from WT and AK β-cells, and the abundances of sphingomyelin molecular species were analyzed by ESI/MS/MS in the presence of 14:0/14:0-GPC (*m/z* 684) internal standard. The WT (*A*) and AK (*B*) spectra were obtained by monitoring constant neutral loss of 59. *C*, total sphingomyelin pool. Content of each sphingomyelin molecular species (pmol) was determined in each group and normalized to total phosphate (μmol of PO_4). The means ± S.E. ($n = 3$) of the total (pmol/μmol of PO_4) sphingomyelin pools are presented. *, AK group significantly different from WT, $p < 0.05$.

(42) in an NSMase-dependent manner, we examined whether there was a similar compromising of ΔΨ in the Akita cells. As in the earlier study, we used a flow cytometry protocol to monitor ΔΨ in a suspension of cells to which a fluorescent Mito Flow reagent was added. This reagent concentrates in the mitochondria of healthy cells, but the mitochondria of cells undergoing apoptosis become compromised and accumulate less of the reagent, and this is reflected by a decrease in the fluorescence signal and the appearance of a second peak that is left of the original. The spectra presented in Fig. 3*A* reflect fluorescence measurement in 10,000 cells, and the percentage of cells (mean of four separate experiments) losing ΔΨ was analyzed by the application software and is indicated as *M1*. These analyses revealed that a higher percentage of Akita cells have compromised ΔΨ than WT cells under basal conditions. However, unlike the INS-1 cells, the Akita and corresponding WT cells were found to be prone to clumping. This resulted in broader peaks in the spectra and an unexpectedly higher *M1* value, even in the WT cells. We therefore established a second protocol in which mitochondria-associated $DiOC_6(3)$ staining (*green*) was monitored in live cells by confocal microscopy. As seen in Fig. 3*B*, $DiOC_6(3)$ under basal conditions is more significantly retained in the mitochondria of WT than in Akita cells, confirming compromised mitochondrial integrity in the Akita cells. Further, Hoechst staining (*blue*) reveals that the nuclei in Akita cells are irregular in shape and size, as compared with the nuclei in WT cells, suggesting that the cell death process is under way in the Akita cells. These findings suggest that the spontaneous development of ER stress in β-cells also triggers the mitochondrial apoptotic pathway.

Basal and ER Stress-induced Apoptosis Are Amplified in Akita β-Cells—In view of the above findings, we next examined if the Akita cells are more susceptible to apoptosis. TUNEL analyses (Fig. 4*A*) revealed a higher incidence of basal apoptosis that was coincident with higher levels of activated caspase-3 (Fig. 4, *B* and *C*). Exposure to thapsigargin induced activation of caspase-3 in both wild type and Akita with peak activation achieved earlier in the Akita cells than in the wild type cells. This is reflected by a greater -fold increase, relative to basal, in Akita cell apoptosis at 8 h (WT, 1.59 ± 0.09 *versus* Akita (AK), 2.26 ± 0.16, $p = 0.0175$).

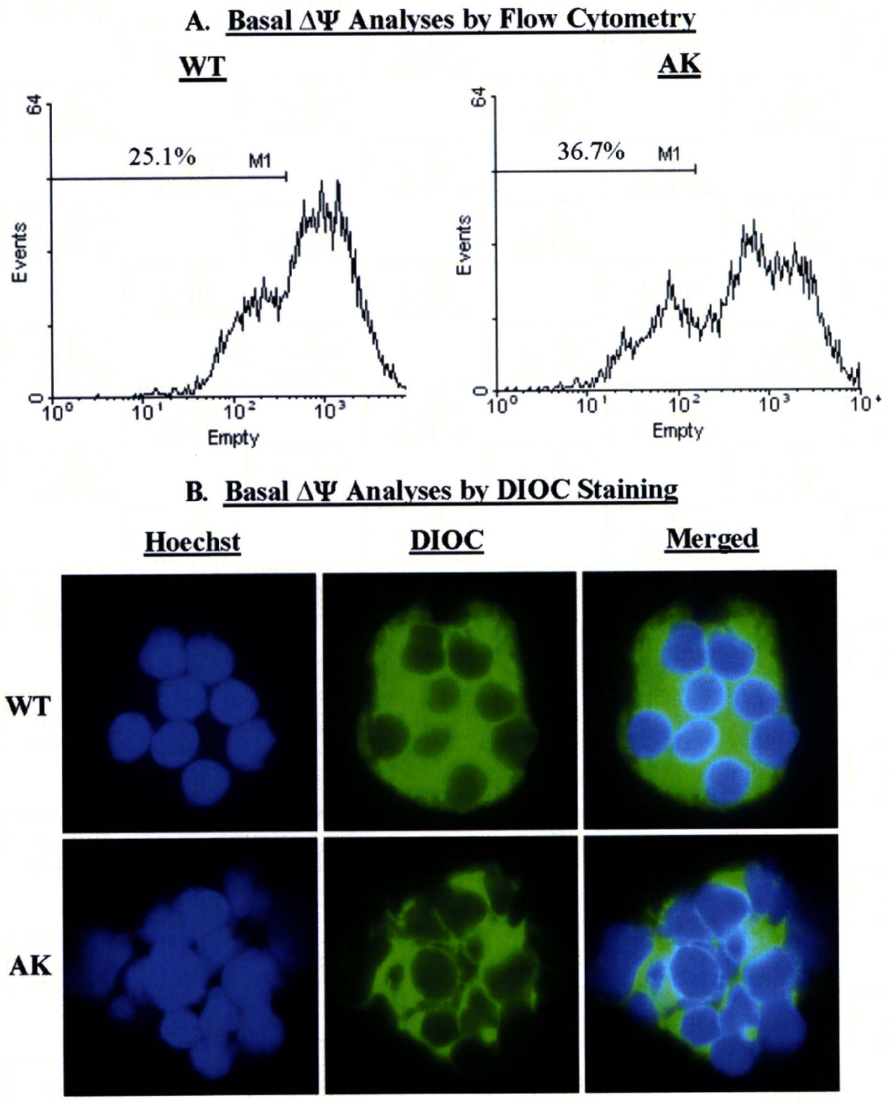

FIGURE 3. **Basal mitochondrial membrane potential (ΔΨ) monitoring.** ΔΨ was monitored in WT and AK β-cells by flow cytometry and DiOC$_6$(3) staining. *A*, flow cytometry. The spectra reflect fluorescence measurement in 10,000 cells, and the percentage of cells losing ΔΨ is indicated as *M1*. These analyses were done four separate times. *B*, DiOC$_6$(3) staining. Cells were loaded with the *blue* nuclear (Hoechst; *left panels*) and *green* mitochondrial (DiOC$_6$(3) (*DIOC*); *middle panels*) stain and examined by confocal microscopy. The *merged images* are shown in the *right panels*.

ER Stress Amplifies ΔΨ Loss in Akita β-Cells—Because induction of ER stress led to mitochondrial abnormalities in the INS-1 cells, we examined whether a similar affect was evident in the Akita cells. Compared with basal conditions (Fig. 2*B*), exposure to thapsigargin for 8 h resulted in dispersion of DiOC$_6$(3) staining and loss in nuclear uniformity in the WT cells (Fig. 4*D*). These outcomes were accelerated in the Akita cells and suggest that activation of the mitochondrial apoptotic pathway contributes to ER stress-induced apoptosis of these cells also.

Expression and ER Stress-induced Activation of iPLA$_2\beta$ and NSMase—Our collective observations (40–42) indicate that ER stress-induced apoptosis occurs by an iPLA$_2\beta$-dependent mechanism involving induction of NSMase and activation of the mitochondrial apoptotic pathway. The above findings suggest participation of both NSMase and the mitochondria in Akita β-cell death. We therefore examined the extent of the iPLA$_2\beta$ role in this process. Surprisingly, basal expression of iPLA$_2\beta$ protein was found to be greater in the Akita than in the WT cells (Fig. 5*A*), and this was reflected by a 3-fold higher activity (16 ± 1 pmol/mg of protein/min for WT *versus* 54 ± 3 pmol/mg of protein/min for Akita). Also, as shown in Fig. 5*B*, exposure to thapsigargin promoted iPLA$_2\beta$ activity in both WT and AK β-cells. Consistent with manifestation of an iPLA$_2\beta$ activity, basal and thapsigargin-treated activities were suppressed by BEL and stimulated by ATP (~3-fold) in WT and AK β-cells.

Because we previously reported iPLA$_2\beta$-mediated induction of NSMase during ER stress, we compared its message levels in the WT and Akita cells. As shown in Fig. 5*C*, basal NSMase was higher in the Akita than in the WT cells, and exposure to thapsigargin induced NSMase. The increase in NSMase message occurred earlier and reached a higher -fold increase in the Akita cells, relative to WT cells. Consistent with an iPLA$_2\beta$-mediated effect, NSMase induction in both groups was inhibited by inactivation of iPLA$_2\beta$ with BEL.

In contrast with the earlier observations in INS-1 cells, in which iPLA$_2\beta$ was overexpressed (41, 42) and the cells were treated with thapsigargin, the responses described here in the Akita β-cells occurred in a spontaneous ER stress model. The present findings therefore strengthen the likelihood that iPLA$_2\beta$ plays a critical role in ER stress-induced β-cell apoptosis.

Evidence for Induction of iPLA$_2\beta$ by SREBP-1 during ER Stress—The finding of increased iPLA$_2\beta$ expression in the Akita cells suggests that the β-cell iPLA$_2\beta$ may be subject to regulation, but the mechanism for its induction remains to be elucidated. One potential possibility is suggested by the recent report identifying a sterol-regulatory element (SRE) in the iPLA$_2\beta$ gene (53). That study performed in Chinese hamster ovary cells revealed that binding of SREBPs to SRE leads to iPLA$_2\beta$ transcription. Of relevance to our interests is that SREBPs are known to be induced under stressful conditions and processed to the mature form of SREBPs (mSREBP) in β-cells experiencing ER stress due to glucolipotoxicity and thapsigargin (54). Consistent with these observations, we find that basal expression of mSREBP-1 protein is greater in Akita than in WT cells (Fig. 6*A*). Further, Akt phosphorylation, which promotes SREBP-1 processing

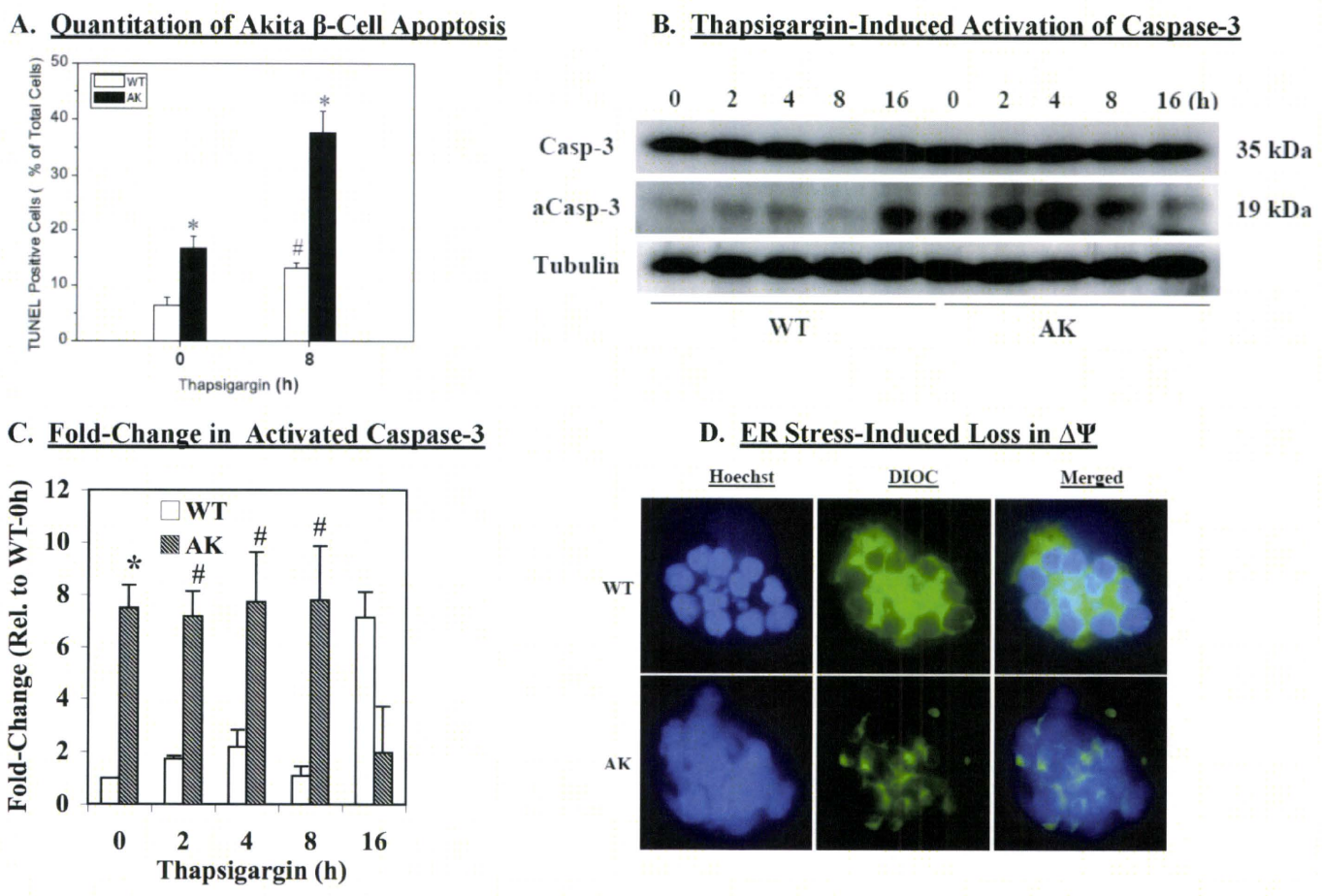

FIGURE 4. **Assessment of apoptosis and mitochondrial membrane potential (ΔΨ) in Akita β-cells.** WT and AK β-cells were exposed to DMSO (control) or thapsigargin (*T*) (0.50 μM) and harvested at various times for analyses. *A*, apoptosis quantitation. Total cell number was determined using DAPI nuclear stain, and the mean ± S.E. ($n = 3$) percentages of TUNEL-positive apoptotic cells are presented. *, AK group significantly different from WT, $p < 0.05$. #, WT treated group significantly different from WT control group, $p < 0.05$. *B*, caspase-3 activation. Cell lysates were prepared and processed for full-length and activated caspase-3 (*Casp-3* and *aCasp-3*, respectively) immunoblotting analyses. Tubulin was used as a loading control. These analyses were done three separate times. *C*, activated caspase-3 densitometry. The ratio of the activated caspase-3-immunoreactive band to the corresponding tubulin band was determined, and means ± S.E. of -fold change relative to WT at 0 h are presented. * and #, significantly different from corresponding WT; $p < 0.01$ and $p < 0.05$, respectively. *D*, ΔΨ analyses. Following exposure to DMSO or thapsigargin for 8 h, the WT and AK β-cells were loaded with the blue nuclear (Hoechst) (*left panels*) and green mitochondrial ($DiOC_6(3)$) (*DIOC*) (*middle panels*) stains and examined by confocal microscopy. The *merged images* are shown in the *right panels*.

and nuclear accumulation of the mSREBP-1 (55–57), is also increased.

To determine if there is a link between SREBP-1 and iPLA$_2$β expression, cells were treated with thapsigargin and harvested at various times for immunoblotting analyses. Exposure to thapsigargin promoted a temporal increase in iPLA$_2$β expression in both WT and Akita cells (Fig. 6*B*), with a more pronounced and earlier increase apparent in the Akita cells. Also, as seen in Fig. 6*C*, corresponding increases in mSREBP-1 and pAkt are also evident. These findings reveal a correlation between iPLA$_2$β and generation of SREBP-1; however, they do not indicate whether the increase in iPLA$_2$β expression is due to SREBP-1 processing.

To address a direct role of SREBP-1 on iPLA$_2$β induction, we expressed a DN form of SREBP-1 in the WT and Akita cells. It has been reported that although the DN form itself is unable to activate transcription, it interferes with the processing of endogenous SREBP-1 and its binding to the SRE element (49). As seen in Fig. 6*D*, expression of the DN SREBP-1 reduced basal levels of the mSREBP-1 form and its increase following exposure to thapsigargin. In association with the reduction in mSREBP-1, both basal and thapsigargin-induced increases in iPLA$_2$β were suppressed in cells expressing the DN SREBP-1 (Fig. 6*E*). As expected by the upstream role of pAkt in SREBP-1 activation, phosphorylation of Akt was unaffected by DN SREBP-1 (data not shown). These findings are taken to indicate that SREBP-1 activation can promote iPLA$_2$β expression.

Effects of iPLA$_2$β Knockdown in the Akita Cells—Because basal iPLA$_2$β is increased in the Akita cells that are predisposed to developing ER stress and is induced in both WT and Akita cells following exposure to thapsigargin, we next examined whether suppression of iPLA$_2$β expression prevents the observed outcomes. To address this issue, we used siRNA protocols to knockdown iPLA$_2$β in the WT and Akita cells. The cells were harvested under basal conditions or following an 8-h exposure to thapsigargin. As illustrated in Fig. 7*A*, both basal and thapsigargin-induced iPLA$_2$β protein expression are reduced in the WT and Akita cells transfected with the iPLA$_2$β siRNA (*si*), relative to cells transfected with the control siRNA (*si**). Comparison of iPLA$_2$β message in the control siRNA-transfected WT and Akita cells revealed nearly 2.5-fold higher basal iPLA$_2$β message in the Akita cells (Fig. 7*B*). Transfection